# Metastability of solitary roll wave solutions of the St. Venant equations with viscosity

Blake Barker, Mathew A. Johnson, Luis Miguel Miguel Rodrigues, Kevin Zumbrun

# Metastability of solitary roll wave solutions of the St. Venant equations with viscosity

Blake Barker* Mathew A. Johnson† L.Miguel Rodrigues‡ Kevin Zumbrun§

March 9, 2011

**Keywords**: solitary waves; St. Venant equations; convective instability.

**2000 MR Subject Classification**: 35B35.

**Abstract**

We study by a combination of numerical and analytical Evans function techniques the stability of solitary wave solutions of the St. Venant equations for viscous shallow-water flow down an incline, and related models. Our main result is to exhibit examples of metastable solitary waves for the St. Venant equations, with stable point spectrum indicating coherence of the wave profile but unstable essential spectrum indicating oscillatory convective instabilities shed in its wake. We propose a mechanism based on "dynamic spectrum" of the wave profile, by which a wave train of solitary pulses can stabilize each other by de-amplification of convective instabilities as they pass through successive waves. We present numerical time evolution studies supporting these conclusions, which bear also on the possibility of stable periodic solutions close to the homoclinic. For the closely related viscous Jin-Xin model, by contrast, for which the essential spectrum is stable, we show using the stability index of Gardner–Zumbrun that solitary wave pulses are always exponentially unstable, possessing point spectra with positive real part.

## 1 Introduction

Roll waves are a well-known phenomenon occurring in shallow water flow down an inclined ramp, generated by competition between gravitational force and friction along the bottom.

*Indiana University, Bloomington, IN 47405; bhbarker@indiana.edu: Research of B.B. was partially supported under NSF grants no. DMS-0300487 and DMS-0801745.

†Indiana University, Bloomington, IN 47405; matjohn@indiana.edu: Research of M.J. was partially supported by an NSF Postdoctoral Fellowship under NSF grant DMS-0902192.

‡Université de Lyon, Université Lyon 1, Institut Camille Jordan, UMR CNRS 5208, 43 bd du 11 novembre 1918, F - 69622 Villeurbanne Cedex, France; rodrigues@math.univ-lyon1.fr: Stay of M.R. in Bloomington was supported by Frency ANR project no. ANR-09-JCJC-0103-01.

§Indiana University, Bloomington, IN 47405; kzumbrun@indiana.edu: Research of K.Z. was partially supported under NSF grants no. DMS-0300487 and DMS-0801745.

Such patterns have been used to model phenomena in several areas of the engineering literature, including landslides, river and spillway flow, and the topography of sand dunes and sea beds and their stability properties have been much studied numerically, experimentally, and by formal asymptotics; see [BM] and references therein. Mathematically, these can be modeled as traveling-wave solutions of the St. Venant equations for shallow water flow; see [D, N1, N2] for discussions of existence in the inviscid and viscous case. They may take the form either of periodic wave-trains or, in the long-wavelength limit of such wavetrains, of *solitary pulse-type waves*.

Stability of periodic roll waves has been considered recently in [N1, N2, JZN]. Here, we consider stability of the limiting solitary wave solutions. This appears to be of interest not only for its relation to stability of nearby periodic waves (see [GZ, OZ1] and discussion in [JZN]), but also in its own right. For, persistent solitary waves are a characteristic feature of shallow water flow, but have been more typically modeled by dispersive equations such as Boussinesq or KdV.

Concerning solitary waves of general second-order hyperbolic-parabolic conservation or balance laws such as those examined in this paper, all results up to now [AMPZ1, GZ, Z2] have indicated that such solutions exhibit unstable point spectrum. Thus, it is not at all clear that an example with stable point spectrum should exist. Remarkably, however, for the equations considered in [N2, JZN] we obtain examples of solitary wave solutions that are *metastable* in the sense that they have stable point spectrum, but unstable essential spectrum of a type corresponding to convective instability. That is, the perturbed solitary wave propagates relatively undisturbed down the ramp, while shedding oscillatory instabilities in its wake, so long as the solution remains bounded by an arbitrary constant. The shed instabilities appear to grow exponentially forming the typical time-exponential oscillatory Gaussian wave packets associated with essential instabilities; see the stationary phase analysis in [OZ1]. Presumably these would ultimately blow up according to a Ricatti equation in the standard way; however, for sufficiently small perturbation, this would be postponed to arbitrarily long time. For the time length considered in our numerics, we cannot distinguish between the linear and nonlinear growth.

We confirm this behavior numerically by time evolution and Evans function analysis. We derive also a general stability index similarly as in [GZ, Z2, Go, Z4] counting the parity of the number of unstable eigenvalues, hence giving rigorous geometric necessary conditions for stability in terms of the dynamics of the associated traveling-wave ODE; see Section 3.3. Using the stability index, we show that homoclinics of the closely related viscous Jin–Xin model are *always unstable*; see Section 3.4. We point out also an interesting and apparently so far unremarked connection between the stability index, a Melnikov integral for the homoclinic orbit with respect to variation in the wave speed, and geometry of bifurcating limit cycles (periodic orbits), which leads to a simple and easily evaluable rule of thumb connecting stability of homoclinic orbits as traveling wave solutions of the associated PDE to stability of an enclosed equilibrium as a solution of the traveling-wave ODE; see Remark 3.14.

The examples found in this paper are notable as the first examples of a solitary-wave

solution of a second-order hyperbolic–parabolic conservation or balance law for which the point spectrum is stable. This raises the very interesting question whether an example could exist with both stable point and essential spectrum, in which case linearized and nonlinear orbital stability (in standard, not metastable sense) would follow in standard fashion by the techniques of [MaZ1, MaZ4, Z2, JZ, JZN, LRTZ, TZ1]. In Section 5 we present examples for various modifications of the turbulent friction parameters (different from the ones in [N2, JZN]) that have stable point spectrum and "almost-stable" essential spectrum, or stable essential spectrum and "almost-stable" point spectrum, suggesting that one could perhaps find a spectrally stable example somewhere between. However, we have up to now not been able to find one for the class of models considered here. Whether this is just by chance, or whether the conditions of stable point spectrum and stable essential spectrum are somehow mutually exclusive[1] is an extremely interesting open question, especially given the fundamental interest of solitary waves in both theory and applications.

Finally, we note that similar metastable phenomena have been observed by Pego, Schneider, and Uecker [PSU] for the related fourth-order diffusive Kuramoto-Sivashinsky model

$$u_t + \varepsilon\partial_x^4 u + \partial_x^3 u + \varepsilon\partial_x^2 u + \frac{\partial_x u^2}{2} = 0, \qquad \varepsilon << 1, \tag{1.1}$$

an alternative, small-amplitude, model for thin film flow down an incline. They describe asymptotic behavior of solutions of this model observed in numerical simulations as dominated by trains of solitary pulses, going on to state: "Such dynamics of surface waves are typical of observations in the inclined film problem [CD], both experimentally and in numerical simulations of the free-boundary Navier–Stokes problem describing this system." Yet, as in the present setting, such solitary pulses are necessarily unstable, due to unstable essential spectra coming from the long-wave instability of their limiting constant states, the latter deriving in turn from the destabilizing second-order term $\varepsilon\partial_x^2 u$.

That is, both our results and the results of [PSU] seem to illustrate a larger and somewhat surprising phenomenon, deriving from physical inclined thin-film flow, of asymptotic behavior dominated by trains of pulse solutions which are themselves unstable. Pego, Schneider, and Uecker rigorously verify this phenomenon for (1.1) in the small-amplitude ($\varepsilon \to 0$) limit, showing that solutions starting within $O(1)$ distance of $N$-pulse solutions of the $\varepsilon = 0$ KdV equations remain $O(1)$ close up to time $O(1/\varepsilon)$. However, our results, and the results of numerics and experiment [CD], suggest that this is a much more general phenomenon, not necessarily confined to small amplitudes or even particularly thin films.

We discuss this interesting issue, and the relation to stability of periodic waves, in Section 6, suggesting a heuristic mechanism by which convectively unstable solitary waves- not necessarily of small amplitude- can stabilize each other when placed in a closely spaced array, by de-amplification of convected signals as they cross successive solitary wave profiles. We quantify this by the concept of "dynamic spectrum" of a solitary wave, defined as the spectrum of an associated wave train obtained by periodic extension, appropriately defined, of a solitary wave pulse. In some sense, this notion captures the essential spectrum of the

[1] For a similar dichotomy in a related, periodic context, see [OZ1].

*non-constant* portion of the profile. This is in contrast to usual notion of essential spectrum which is governed by the (often unstable) constant limiting states.

For the waves studied here, the dynamic spectrum is stable, suggesting strongly that long-wave periodic trains are stable as well. This conjecture has since been verified in [BJNRZ1, BJNRZ2]. However, we emphasize that the dynamic spectrum has importance also apart from the discussion of periodic waves, encoding properties of a solitary wave even in the absence of nearby periodics: specifically, the extent to which perturbations are amplified or de-amplified as they cross the main portion of the wave.

**Acknowledgement**: Thanks to Björn Sandstede for pointing out the reference [PSU], to Bernard Deconink for his generous help in guiding us in the use of the SpectrUW package developed by him and collaborators, and to Pascal Noble for helpful discussions and for his ongoing collaboration on related projects. K.Z. thanks Björn Sandstede and Thierry Gallay for interesting conversations regarding stabilization of unstable arrays, and thanks the Universities of Paris 7 and 13 for their warm hospitality during a visit in which this work was partly carried out. The numerical Evans function computations performed in this paper were carried out using the STABLAB package developed by Jeffrey Humpherys with help of the first and last authors; we gratefully acknowledge his contribution. Finally, thanks to the two anonymous referees for helpful suggestions that improved the exposition.

# 2 The St. Venant equations with viscosity

## 2.1 Equations and setup

The 1-d viscous St. Venant equations approximating shallow water flow on an inclined ramp are

$$\begin{aligned} h_t + (hu)_x &= 0, \\ (hu)_t + (h^2/2F + hu^2)_x &= h - u|u|^{r-1}/h^s + \nu(hu_x)_x, \end{aligned} \tag{2.1}$$

where $1 \leq r \leq 2$, $0 \leq s \leq 2$, and where $h$ represents height of the fluid, $u$ the velocity average with respect to height, $F$ is the Froude number, which here is the square of the ratio between speed of the fluid and speed of gravity waves, $\nu = \mathrm{Re}^{-1}$ is a positive nondimensional viscosity equal to the inverse of the Reynolds number, the term $u|u|^{r-1}/h^s$ models turbulent friction along the bottom, and the coordinate $x$ measures longitudinal distance along the ramp. Furthermore, the choice of the viscosity term $\nu(hu_x)_x$ is motivated by the formal derivations from the Navier Stokes equations with free surfaces. Typical choices for $r$, $s$ are $r = 1$ or 2 and $s = 0$, 1, or 2; see [BM, N1, N2] and references therein. The choice considered in [N1, N2, JZN] is $r = 2$, $s = 0$.

Following [JZN], we restrict to positive velocities $u > 0$ and consider (2.1) in Lagrangian coordinates, in which case (2.1) appears as

$$\begin{aligned} \tau_t - u_x &= 0, \\ u_t + ((2F)^{-1}\tau^{-2})_x &= 1 - \tau^{s+1}u^r + \nu(\tau^{-2}u_x)_x, \end{aligned} \tag{2.2}$$

where $\tau := h^{-1}$ and $x$ now denotes a Lagrangian marker rather than physical location. This choice of coordinates was crucial in the analysis of [JZN], which considers the nonlinear stability of periodic traveling wave solutions of (2.1) to small localized perturbations: the Lagrangian form was essential in the development of large-amplitude damping estimates, demonstrating exponential slaving of high-order Sobolev norms to lower-order ones. Continuing this line of investigation then, we choose to work with the governing equation (2.2) throughout this paper as opposed to (2.1).

**Remark 2.1.** Since we study waves propagating down a ramp, there is no real restriction in taking $u > 0$. However, we must remember to discard any anomalous solutions which may arise for which negative values of $u$ appear.

**Remark 2.2.** Equations (2.1) may be derived in a small-depth limit from the corresponding free-boundary surface wave problem for the incompressible Navier–Stokes equations with flat, inclined bottom, neglecting surface tension [BN]. The addition of surface tension would lead to an additional third-derivative term in $\tau$ on the righthand side of the second equation in (2.1), similar to a capillary pressure term in compressible fluid dynamics. Equation (1.1) may be derived from (2.1) in a small-amplitude, near-horizontal limt near transition to instability of constant solutions, or, in the same limit, directly from the Navier–Stokes free-surface problem from which (2.1) was derived: see [W, YKH]. In either case, the dominant third-order (KdV) term in (1.1) arises despite the absence of surface tension in the underlying models, coming rather from the detailed interaction of lower-order terms in the small-amplitude expansion. By contrast, the derivation of (1.1) in the near-vertical scenario described in [CD] corresponds to a Stokes, or infinite-surface tension limit.

We begin by considering the existence of solitary traveling wave solutions of (2.2). Denoting the vector $U := (\tau, u)$, we note that the components of a traveling-wave solution $U = \bar{U}(x - ct)$ of (2.2) are easily seen to satisfy the traveling-wave system of ODE's

$$\begin{aligned} -c\bar{\tau}' - \bar{u}' &= 0, \\ -c\bar{u}' + ((2F)^{-1}\bar{\tau}^{-2})' &= 1 - \bar{\tau}^{s+1}\bar{u}^r + \nu(\bar{\tau}^{-2}\bar{u}')'. \end{aligned} \tag{2.3}$$

The first equation of (2.3) may be directly integrated, yielding $\bar{u}(\bar{\tau}) := q - c\bar{\tau}$ where $q$ is the resulting constant of integration. Substituting this identity into the second equation of (2.3) we obtain the second-order scalar profile equation in the component $\bar{\tau}$ alone:

$$c^2\bar{\tau}' + ((2F)^{-1}\bar{\tau}^{-2})' = 1 - \bar{\tau}^{s+1}(q - c\bar{\tau})^r - c\nu(\bar{\tau}^{-2}\bar{\tau}')'. \tag{2.4}$$

Notice that solutions $\bar{\tau}$ of (2.4) correspond in a bijective fashion with the solutions of (2.3) through the mapping

$$\bar{\tau} \mapsto \begin{pmatrix} \bar{u} \\ \bar{\tau} \end{pmatrix} := \begin{pmatrix} q - c\bar{\tau} \\ \bar{\tau} \end{pmatrix}$$

First, we note that nontrivial traveling-wave solutions of (2.4) with speed $c = 0$ do not exist in Lagrangian coordinates. Indeed, taking $c = 0$ implies that $\bar{u} \equiv q$ in which case (2.4)

reduces to the scalar first-order equation

$$\bar{\tau}' = F\bar{\tau}^3(\bar{\tau}^{s+1}q^r - 1), \tag{2.5}$$

which has no nontrivial solutions with $\bar{\tau} > 0$. Nevertheless, for non-zero values of $c$ it can easily be seen numerically that (2.4) admits homoclinic orbits corresponding to solitary wave solutions of (2.2); see also [N1, N2]. Typically these homoclinic orbits emerge in a two-stage process, starting with a Hopf bifurcation from the equilibrium state as wave speed is varied through a critical value, generating a family of periodic orbits which then grow in amplitude as speed is further varied, terminating finally through a homoclinic bifurcation into a bounding homoclinic: that is, a standard global saddle-node bifurcation configuration. The appearance of periodic waves at least is easy to verify analytically, and we thus continue our analysis by deriving the Hopf bifurcation conditions associated with the profile ODE (2.4), at the same time deriving conditions for stability of constant solutions that will be of later use.

## 2.2 The subcharacteristic condition and Hopf bifurcation

To begin, we consider the stability of the constant solutions of equation (2.2), noting that instability of constant solutions is typically associated with pattern formation and Hopf-bifurcation to periodic orbits. Indeed, neutral time-evolutionary instability of constant solutions is readily seen to be a necessary condition for Hopf bifurcation from the associated equilibrium in the traveling-wave ODE, as appearance of spatially periodic traveling-wave solutions is associated with nontrivial pure imaginary (essential) spectra of the linearized operator about the constant state. This may be seen in general by noting that the variation with respect to amplitude of the bifurcating family of periodic waves is an eigenfunction with imaginary eigenvalue. We give a direct verification below.

First note that (2.2) is of $2 \times 2$ viscous relaxation type and can be written in the form

$$U_t + H(U)_x - \nu(B(U)U_x)_x = \begin{pmatrix} 0 \\ g(U) \end{pmatrix}, \tag{2.6}$$

where $g(U) = 1 - \tau^{s+1}u^r$ and

$$H(U) = \begin{pmatrix} -u \\ \frac{1}{2F\tau^2} \end{pmatrix}, \quad B(u) = \begin{pmatrix} 0 & 0 \\ 0 & \tau^{-2} \end{pmatrix}.$$

At equilibrium values $u = \tau^{-(s+1)/r} > 0$, the inviscid version of (2.6), obtained by setting $\nu = 0$ in (2.6), has hyperbolic characteristics equal to the eigenvalues $\pm\frac{\tau^{-3/2}}{\sqrt{F}}$ of $dH$, and equilibrium characteristic $\left(\frac{s+1}{r}\right)\tau^{-(r+s+1)/r}$ equal to $df_*(\tau)$, where $f_*(\tau) := -u_*(\tau)$ and $u_*(\tau) := \tau^{-(s+1)/r}$ is defined by $g(\tau, u_*(\tau)) = 0$. The subcharacteristic condition, i.e., the condition that the equilibrium characteristic speed lie between the hyperbolic characteristic speeds, is therefore

$$df_*(\tau) = \left(\frac{s+1}{r}\right)\frac{u_*(\tau)}{\tau} = \left(\frac{s+1}{r}\right)\tau^{-(r+s+1)/r} \leq \frac{\tau^{-3/2}}{\sqrt{F}} = c_s(\tau). \tag{2.7}$$

For the common case $r = 2$, $s = 0$ considered in [N2, JZN], this reduces to $F \leq 4$. For $2 \times 2$ relaxation systems such as the above, the subcharacteristic condition is exactly the condition that constant solutions be linearly stable, as may be readily verified by computing the dispersion relation using the Fourier transform.

**Remark 2.3.** *Let $q$ and $c$ be fixed. Then the equilibria of the traveling-wave ODE* (2.4) *are given by zeros of $g_*(\tau) = g(\tau, q - c\tau)$ (corresponding to $u_*(\tau) = q - c\tau$). Notice that the relation $dg_*(\tau) = g_\tau(\tau) - cg_u(\tau) = g_u(\tau)(df_*(\tau) - c)$. Since $g_u < 0$, by the relaxation structure of* (2.6)*, the key quantity $df_* - c$ has a sign opposite to the one of $dg_*$. Therefore, provided there is no multiple root of $g_*$, the sign of $df_*(\tau_0) - c$ alternates among the equilibria $\tau_0$ of the traveling-wave ODE* (2.4)*.*

For the full system (2.6) with viscosity $\nu > 0$, we now show some Fourier computations relating the subcharacteristic condition with both stability of constant states and its necessity for the occurrence of a Hopf bifurcation. Let speed $c$ be fixed. Then rewriting (2.6) in a moving frame $(x - ct, t)$ and linearizing about a constant solution $(\tau, u) \equiv (\tau_0, u_0)$, with $\tau_0 > 0$ and $u_0 = u_*(\tau_0) > 0$, we obtain the linear system $U_t + A_0 U_x = B_0 U + C_0 U_{xx}$, where[2]

$$A_0 = \begin{pmatrix} -c & -1 \\ -c_s^2 & -c \end{pmatrix}, \qquad B_0 = \begin{pmatrix} 0 & 0 \\ -(s+1)/\tau_0 & -r/u_0 \end{pmatrix}, \qquad C_0 = \begin{pmatrix} 0 & 0 \\ 0 & \nu\tau_0^{-2} \end{pmatrix}, \tag{2.8}$$

and $c_s = c_s(\tau_0) = \frac{\tau_0^{-3/2}}{\sqrt{F}}$ denotes the positive hyperbolic characteristic of the inviscid problem (see above). The corresponding dispersion relation between eigenvalue $\lambda$ and frequency $k$ is readily seen to be given by the polynomial equation

$$\begin{aligned} 0 &= \det(\lambda I + A_0 ik - B_0 + k^2 C_0) \\ &= \lambda^2 + \left[\frac{r}{u_0} - 2ick + \frac{\nu k^2}{\tau_0^2}\right]\lambda + ik\left[\frac{s+1}{\tau_0} - \frac{cr}{u_0} + ik(c^2 - c_s^2) - \frac{c\nu k^2}{\tau_0^2}\right]. \end{aligned} \tag{2.9}$$

Inspecting stability, we Taylor expand the dispersion relation (2.9) about an eigenvalue $\lambda$ with $\Re(\lambda) = 0$. Note that if $\lambda$ is such an eigenvalue corresponding to a non-zero frequency $k$, we may assume $\lambda = 0$ by replacing $c$ with $c - \Im(\lambda)/k$. Let us then focus on $k = 0$ or $\lambda = 0$ and $k \neq 0$.

Eigenvalues corresponding to $k = 0$ are 0 and $-r/u_0$. Solving the dispersion equation (2.9) about $(\lambda, k) = (0, 0)$ with $\lambda(k)$ and differentiating, one finds

$$\lambda'(0) = -i\left[\left(\frac{s+1}{r}\right)\frac{u_0}{\tau_0} - c\right]$$

and

$$\frac{1}{2}\lambda''(0) = \frac{u_0}{r}\left[\big(i\lambda'(0) + c\big)^2 - c_s^2\right] = \frac{u_0}{r}\left[\left(\left(\frac{s+1}{r}\right)\frac{u_0}{\tau_0}\right)^2 - c_s^2\right].$$

[2]Recall that $\tau_0^{s+1} u_0^r = 1$.

so that failure of the subcharacteristic condition implies spectral instability. Furthermore, it follows that any solitary wave solution of (2.2) for which the limiting value $\lim_{x\to\pm\infty}\tau(x)$ violates the subcharacteristic condition (2.7) will have unstable essential spectrum.

We now look for eigenvalues $\lambda = 0$ for $k \neq 0$ by solving

$$0 = \frac{s+1}{\tau_0} - \frac{cr}{u_0} + ik(c^2 - c_s^2) - \frac{c\nu k^2}{\tau_0^2}. \tag{2.10}$$

Such a $k$ exists if and only if $c = c_s$ and $\left(\frac{s+1}{r}\right)\frac{u_0}{\tau_0} > c_s$, and then the solutions are $\pm k_H$ with

$$k_H = \sqrt{\frac{\tau_0^2 r}{c_s \nu u_0}\left[\left(\frac{s+1}{r}\right)\frac{u_0}{\tau_0} - c_s\right]}.$$

Now, solving the dispersion equation (2.9) about $(\lambda, k) = (0, \pm k_H)$ with $\lambda(k)$ and differentiating, one finds

$$\lambda'(\pm k_H) = \frac{2c_s\nu}{\tau_0^2}\frac{ik_H^2}{r/u_0 + \nu k_H^2/\tau_0^2 \mp 2ic_s k_H} \notin i\mathbb{R} \tag{2.11}$$

yielding again instability. See Figure 1 for a typical depiction of the triple degeneracy of the essential spectrum at $\lambda = 0$ for an unstable constant state when $c = c_s$.

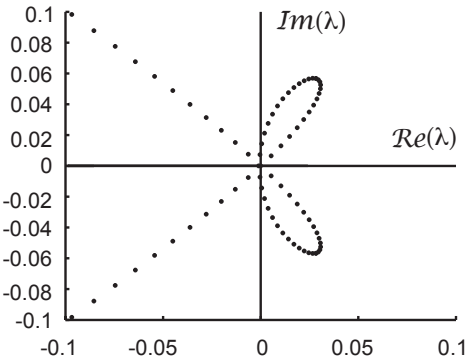


Figure 1: Here, we depict a numerical sampling of the (continuous) essential spectrum of the PDE (2.6), plotted as $\Re(\lambda)$ vs. $\Im(\lambda)$, when linearized about a constant state, for values of the parameters at which the constant state undergoes a Hopf bifurcation when considered as a fixed point of the ODE (2.4). In this example, we have taken $r = 2$, $s = 4$, $u_0 = 0.96$, $q = u_0 + c/u_0^2$, $\nu = 0.1$, $F = 6$, and $c = c_s = 0.57052639$ (corresponding to the Hopf bifurcation). Notice the triple degeneracy of the $\lambda = 0$ eigenvalue in this case.

Actually equation (2.10) is the linearization of the profile equation (2.4) (with $q = u_0 + c\tau_0$) about $\tau_0$, expressed in Fourier variables, so that the previous pragraph translates

to the *Hopf bifurcation conditions* for the generalized St. Venant equations (2.2)

$$c = c_s(\tau_0) = \frac{\tau_0^{-3/2}}{\sqrt{F}} \quad \text{and} \quad df_*(\tau_0) > c_s(\tau_0). \tag{2.12}$$

(Since background solutions are contant, not only intersection with, but also transversal crossing by eigenvalues of the imaginary axis is readily verified, completing the Hopf scenario.) Moreover $k_H$ is the limiting frequency associated to the Hopf bifurcation and relation (2.11) will yield instability for close-by periodic traveling-waves generated through the Hopf bifurcation. See [JZN] for an alternate derivation of these bifurcation conditions.

### 2.3 Homoclinic bifurcation

Numerical experiments of [N2, BJNRZ1, BJNRZ2] in case $r = 2$, $s = 0$ indicate that, when $F > 4$, there is a smooth family of periodic waves parameterized by period, which increase in amplitude as period is increased, finally approaching a limiting homoclinic orbit as period goes to infinity; see [N2, BJNRZ1, BJNRZ2]. Likewise, in the study of a related artificial viscosity model with $r = 2$, $s = 0$ [HC], periodic and homoclinic solutions *were found in the regime of unstable constant solutions,* $F > 4$. More precisely, in [HC] the above configuration and generation of the periodic and homoclinic orbits were demonstrated analytically by the study of the saddle-node bifurcation where the nonlinear center and saddle point coalesce. The authors were then able to numerically follow these configurations to obtain a global description of phase space. While it seems possible that a complete existence theory analogous to that in [HC] can be developed in the current real viscosity model, such computations are outside the interests of this paper, and we here just numerically track the bounding homoclinic bifurcation as described in §5. We expect, however, that the necessary modifications would be fairly straightforward.

**Remark 2.4.** Let us further examine the linearized profile equation (2.4). For this equation, if $c(df_*(\tau_0) - c) < 0$ then the equilibrium $\tau_0$ is a saddle point ; whereas if $c(df_*(\tau_0) - c) > 0$ then if $c(c^2 - c_s(\tau_0)^2) < 0$ the equilibrium $\tau_0$ is a repeller, either of spiral or real type, and if $c(c^2 - c_s(\tau_0)^2) > 0$ the equilibrium $\tau_0$ is an attractor, either of spiral or real type. In particular, by the alternating property, the repeller case describes behavior at a single equilibrium $\tau_1$ trapped within a homoclinic (asymptotic to $\tau_0$) if and only if there stands $c(c^2 - c_s(\tau_1)^2) < 0$. For the example wave considered in Section 5 we have $r = 2$, $s = 0$, $c = .78$, $F = 6$, $q = 1.78$, $\tau_0 = 1$ and $c_s(\tau_0) = 1/\sqrt{2F} < .289 < .78$ at the saddle equilibrium, but, at the enclosed equilibrium $\tau_1 < 1/2$, $c_s(\tau_1) = \tau_1^{-3/2}/\sqrt{2F} > .816 > .78$.

## 3 Analytical stability framework

### 3.1 Linearized eigenvalue equations and convective instability

We now begin our study of the stability of a given homoclinic solution $U(x,t) = \bar{U}(x - ct)$ satisfying $\lim_{x\to\pm\infty} = U_0$ to localized perturbations in $L^2(\mathbb{R};\mathbb{R}^2)$. To this end, notice that

changing to co-moving coordinates, linearizing about $\bar{U} = (\bar{\tau}, \bar{u})$, and taking the Laplace transform in time we obtain the linearized eigenvalue equations

$$\begin{aligned} \lambda\tau - c\tau' - u' &= 0, \\ \lambda u - cu' - (\bar{\tau}^{-3}(F^{-1} - 2\nu\bar{u}_x)\tau)' &= -(s+1)\bar{\tau}^s\bar{u}^r\tau - r\bar{\tau}^{s+1}\bar{u}^{r-1}u + \nu(\bar{\tau}^{-2}u')'. \end{aligned} \tag{3.1}$$

As we are considering localized perturbations, we consider the $L^2$ spectrum of the eigenvalue equations (3.1). Further, we say the underlying solitary wave $\bar{U}$ is spectrally stable provided that the $L^2$ spectrum of (3.1) lies in the stable half plane $\{\Re\lambda \leq 0\}$ and is spectrally unstable otherwise.

In order to analyze the spectral stability of the underlying solution $\bar{U}$, we consider the point and essential spectrum of the linearized equations (3.1) separately. Here, we define the point spectrum in the generalized sense of [PW2] (including also resonant poles) as zeros of an associated Evans function (description just below), and stability of the point spectrum as nonexistence of such zeros with nonnegative real part, other than a single translational eigenvalue always present at frequency $\lambda = 0$. Equivalently [Sat], this notion of generalized point spectrum can be described in terms of usual eigenvalues of the linearized operator with respect to an appropriate weighted norm; see [TZ2] for further discussion. Furthermore, we define the essential spectrum in the usual complementary sense: that is, as the relative complement of the point spectrum (in the generalized sense described above) in the $L^2$ spectrum of the linearized equations (3.1).

Concerning the structure of the essential spectrum, we recall a classical theorem of Henry [He, GZ] which states that the essential spectrum of the linearized operator (3.1) about the wave both includes and is bounded to the right in the complex plane by the right envelope of the union of the essential spectra of the linearized operators about the constant solutions corresponding to the left and right end states $\lim_{x\to\pm\infty} U(x)$, which in our case agree with the common value $U_0$. This in turn may be determined by a Fourier transform computation as in Section 2.2. Consulting our computations in Section 2.2, we see that in the common case $r = 2$, $s = 0$ constant solutions are *unstable* in the region of existence of solitary waves, and hence solitary waves in this case always have *unstable essential spectrum* (see discussion, Section 2.3), and hence are linearly unstable with respect to standard (e.g., $L^p$ or $H^s$) norms.

As discussed in [PW2, Sat], however, such instabilities are often of "convective" nature, meaning that growing perturbations are simultaneously swept away from, or "radiated" from the solitary wave profile, which itself remains, at least to linear order, intact. This corresponds to the situation that generalized point spectrum, governing near-field behavior, is stable, while essential spectrum, governing far-field behavior is unstable. The phenomenon of convective instability can be captured at a linearized level by the introduction of an appropriate weighted norm [Sat, PW1], with respect to which the essential spectrum is shifted into the negative half-plane and waves are seen (by the Hille–Yosida Theorem) to be linearly time-exponentially stable. Alternatively, see the pointwise description obtained by stationary phase estimates in [OZ1] of the far-field behavior as of an oscillatory time-exponentially growing Gaussian wavepacket convected with respect to the wave. (See also

[AMPZ2].)

Next, we continue our discussion by developing the necessary tools to analyze the point spectrum of (3.1). Notice that, as stated in the introduction, spectral stability of *both* point and essential spectrum, should it occur, can be shown to imply linearized and nonlinear stability in the standard time-asymptotic sense by the techniques of [MaZ1, MaZ3, MaZ4, LRTZ, TZ1, JZN]. However, as also noted in the introduction, we have so far not found a case in which these conditions coexist.

## 3.2 Construction of the Evans function

In order to describe the point spectrum (defined above in the generalized sense), we outline here the construction of the Evans function corresponding to the linearized eigenvalue equations (3.1). First, notice that setting $W := (\tau, u, \bar\tau^{-2}u')^T$, and recalling that $\bar u = (q - c\bar\tau)$, we may write (3.1) as a first-order system of the form $W' = A(x,\lambda)W$, suitable for an Evans function analysis, where

$$A := \begin{pmatrix} \lambda/c & 0 & -\bar\tau^2/c \\ 0 & 0 & \bar\tau^2 \\ \frac{(s+1)\bar\tau^s(q-c\bar\tau)^r - \bar\alpha_x - \bar\alpha\lambda/c}{\nu} & \frac{\lambda + r\bar\tau^{s+1}(q-c\bar\tau)^{r-1}}{\nu} & \frac{-c\bar\tau^2 + \bar\alpha\bar\tau^2/c}{\nu} \end{pmatrix}, \tag{3.2}$$

$$\bar\alpha := \bar\tau^{-3}(F^{-1} + 2c\nu\bar\tau_x), \qquad \bar\alpha_x = -3\bar\tau^{-4}\bar\tau_x(F^{-1} + 2c\nu\bar\tau_x) + 2\bar\tau^{-3}c\nu\bar\tau_{xx}. \tag{3.3}$$

As with the essential spectrum, the study of the point spectrum starts by analyzing the behavior of the system (3.2) evaluated at the constant end state $U_0$ of the underling solitary wave. To begin, we make the following standard definition extending the notion of hyperbolicity of the limiting constant-coefficient system at $\pm\infty$ associated with first-order system (3.2).

**Definition 3.1.** *Following [AGJ, GZ], for a generalized eigenvalue equation $W' = A(x,\lambda)W$, with*

$$\lim_{x\to\pm\infty} A(x,\lambda) = A_0(\lambda),$$

*we define the* region of consistent splitting *to be the connected component of real plus infinity*[3] *of the set of $\lambda$ such that $A_0$ has no center subspace, that is, the stable and unstable subspaces $\mathcal{S}(A_0)$ and $\mathcal{U}(A_0)$ of $A_\pm$ are of constant dimensions summing to the dimension of the entire space and maintain a spectral gap with respect to zero.*

We say that an eigenvalue problem satisfies consistent splitting if the region of consistent splitting includes the entire punctured unstable half-plane $\{\lambda \,|\, \Re\lambda \geq 0\}\backslash\{0\}$ of interest in the study of stability.[4] The notion of consistent splitting contains all the necessary information in order to define an Evans function. Furthermore, the notion of consistent splitting has an immediate consequence concerning the stability of the limiting end states.

[3] Throughout our analysis, we refer to the extended complex number $\lambda = +\infty + 0i$ as real plus infinity.

[4] Recall, [GZ, MaZ3, JZN], that the special point $\lambda = 0$ may be adjoined by analytic extension.

**Lemma 3.2** ([AGJ, GZ, MaZ3])**.** *Consistent splitting is equivalent to spectral stability of the constant solution $U \equiv U_0$, defined as nonexistence of spectra of the constant-coefficient linearized operator about $U_0$ on the punctured unstable half-plane $\{\lambda \,|\, \Re\lambda \geq 0\} \setminus \{0\}$.*

*Proof.* This follows from the standard observation [GZ, ZH, MaZ3, Z1] that the set of $\lambda$ for which $A_0(\lambda)$ possesses a pure imaginary eigenvalue $\mu = ik$ is given by the linear dispersion relations $\lambda = \lambda_j(k)$ for the associated constant-coefficient equation $U_t = LU := BU_{xx} - AU_x + CU$, defined by the roots of $\det(\lambda I - k^2 B - ikA + C) = 0$. □

In the common case $r = 2$, $s = 0$, the Fourier transform computations of Section 2.2 show that constant solutions are unstable in the regime of existence of homoclinic orbits[5] and thus consistent splitting must fail in this case. Thus, while the notion of consistent splitting is sufficient for the construction of an Evans function, it is insufficient for our purposes. For our applications then, we need a generalization of the notion of consistent splitting which still incorporates the essential features necessary for the construction of an Evans function. Such a generalization was observed in [PW2], which we now recall.

**Definition 3.3.** *Following [PW2], we define the* extended region of consistent splitting *to be the largest connected superset of the region of consistent splitting on which the total eigenspaces associated with the stable (resp. unstable) subspaces of $A_0$ maintain a spectral gap* with respect to each other*, that is, for which the eigen-extensions $\hat{\mathcal{S}}$ and $\hat{\mathcal{U}}$ of the stable and unstable subspaces $\mathcal{S}(A_0)$ and $\mathcal{U}(A_0)$ defined for $\lambda$ near real plus infinity satisfy the condition that the maximum real part of eigenvalues of $\hat{\mathcal{S}}$ is strictly smaller than the minimum real part of of eigenvalues of $\hat{\mathcal{U}}$.*

We say that an eigenvalue problem satisfies extended consistent splitting if the region of extended consistent splitting includes the entire punctured unstable half-plane $\{\lambda | \Re\lambda \geq 0\} \setminus \{0\}$. Notice that the Fourier transform computations of Section 2.2 show that extended consistent splitting holds in a neighborhood of the origin[6] in the common case $r = 2$, $s = 0$ while, as mentioned above, consistent splitting does not. Next, under the assumption of extended consistent splitting we show that it is possible to relate the large $x$ behavior of the first order system $W' = A(x, \lambda)W$, with $A$ given as in (3.2), to the behavior of limiting system $W' = A_0(\lambda)W$, where the coefficient matrix $A_0$ is defined as above.

**Lemma 3.4** ([GZ, ZH, Z1])**.** *Let $A(x, \lambda)$ be analytic in $\lambda$ as a function into $C^0(x)$, exponentially convergent to $A_0$ as $x \to \pm\infty$, and satisfying extended consistent splitting. Then, there exist globally defined bases $\{W_1^-, \dots, W_l^-\}$ and $\{W_{l+1}^+, \dots, W_n^+\}$, analytic in $\lambda$ on $\{\Re\lambda \geq 0\} \setminus \{0\}$, spanning the manifold of solutions of $W' = A(x, \lambda)W$ approaching exponentially in angle as $x \to -\infty$ (resp. $x \to +\infty$) to $\hat{\mathcal{U}}(A_0)$ and $\hat{\mathcal{S}}(A_0)$, where $l = \dim\hat{\mathcal{U}}(A_0)$*

[5] At least, for those generated through a Hopf bifurcation. Recall, however, that all homoclinic orbits studied here are obtained in this way.

[6] Away from the origin, extended consistent splitting can be checked numerically in the course of performing the Evans function computations outlined in Section 5. In particular, the numerical code for the Evans computations is written in such a way that failure of extended consistent splitting signals an error.

*and $n = \dim U$; more precisely,*

$$W_j^{\pm} \sim e^{\pm A_0 x} V_j^{\pm} \quad \text{as} \quad x \to \pm\infty \tag{3.4}$$

*for analytically chosen bases $V_j^{\pm}$ of $\hat{\mathcal{U}}(A_0)$ and $\hat{\mathcal{S}}(A_0)$. For the eigenvalue equations considered here, these bases (both $W_j^{\pm}$ and $V_j^{\pm}$) extend analytically to $\Re\lambda \leq -\eta < 0$.*

*Proof.* The first, general result follows by the conjugation lemma of [MeZ] (see description, [Z1]) asserting that exponentially convergent variable-coefficient ODE on a half-line may be converted by an exponentially trivial coordinate transformation to constant-coefficient ODE $Z' = A_0 Z$, together with a lemma of Kato [K, Z6] asserting existence of globally analytic bases $\{V_j^{\pm}\}$ for the range of an analytic projection, the eigenprojections being analytic due to spectral gap. Extension to $\lambda = 0$ (and thus $\Re\lambda \leq -\eta < 0$ for some $\eta$) then follows by a matrix perturbation expansion at $\lambda = 0$ verifying analytic extension of the projectors. See [GZ, MaZ3, Z1] for the now-standard details of this argument. □

By Lemma 3.4 then, solutions of the full linearized system $W' = A(x,\lambda)W$ behave asymptotically like the solutions of the limiting system $W' = A_0(\lambda)W$. Thus, if $\lambda$ is in the point spectrum (in the usual $L^2$ sense) of (3.1) the corresponding vector solution of full linearized system should decay as $x \to \pm\infty$ corresponding to a connection between the stable and unstable subspaces of $A_0$. For the linearized St. Venant eigenvalue equations considered here, computations like those of Section 2.2 show that on the region of consistent splitting the limiting coefficient matrix $A_0(\lambda)$ has a one-dimensional stable subspace[7] and hence Lemma 3.4 applies with $l = 2$ and $n = 3$; as with extended consistent splitting, this is something that can be numerically verified away from $\lambda = 0, \infty$. It follows that $\lambda$ belongs to the point spectrum of (3.1) provided the spaces $\text{span}\{W_1^-, W_2^-\}$ and $\text{span}\{W_3^+\}$ intersect non-trivially, which leads us to our definition of the Evans function.

**Definition 3.5.** *For the linearized St. Venant eigenvalue equations, we define the Evans function as*

$$D(\lambda) := \frac{\det(W_1^-, W_2^-, W_3^+)|_{x=0}}{\det(V_1^-, V_2^-, V_3^+)}, \tag{3.5}$$

*where $V_j^{\pm}$ are the limiting directions of $W_j^{\pm}$. Furthermore, we say $\lambda$ belongs to the point spectrum of* (3.1) *provided $D(\lambda) = 0$.*

**Remark 3.6.** Note that definition (3.5) is independent of the choice of basis elements $V_j^{\pm}$, $W_j^{\pm}$, so long as (3.4) holds. Thus, it is not necessary in practice to choose the $V_j^{\pm}$ analytically, or even continuously. This way of normalizing the Evans function for homoclinics by considering the limiting vectors $V_j^{\pm}$ seems to be not only new to the literature, but also quite convenient for analytical computations; see the calculations below.

[7] This dimension can be found near the origin or near real plus infinity and is, by definition, constant in the region of consistent splitting.

**Remark 3.7.** Note, further, that the Evans function defined for pulse-type (homoclinic) traveling waves in (3.5) is equivalent to the "standard" one $\tilde{D}(\lambda) := \det(W_1^-, W_2^-, W_3^+)|_{x=0}$ prescribed in Definition 4.1, [Z10] for more general front- or pulse-type traveling waves, where $R_- = (V_1^-, V_2^-)$ and $R_+ = (V_3^+)$ are analytically-varying bases determined by Kato's ODE [K, Z6] $R'_\pm = (\Pi\Pi' - \Pi'\Pi)_\pm R_\pm$, with $\Pi_\pm$ the eigenprojections onto the unstable (stable) subspace of $A_\pm = \lim_{x\to\pm\infty} A(x,\lambda)$. For, in the case $A_+ = A_- = A_0$ considered here, $(\Pi\Pi' - \Pi'\Pi)_+ = (\Pi\Pi' - \Pi'\Pi)_-$, and so, by Abel's Lemma, $\det(R_-, R_+)' = \text{Trace}(\Pi\Pi' - \Pi'\Pi)_+ = 0$, and $\det(V_1^-, V_2^-, V_3^+) \equiv$ constant. Thus, $\tilde{D}$ is a constant multiple of $D$, a difference that does not affect either location of zeros or geometry of the map from $\mathbb{C}$ to $D(\mathbb{C})$. The numerical computations of Section 5 are in fact carried out using the version $\tilde{D}$ supported in the numerical Evans package STABLAB. Hereafter we drop the tilde, writing $D$ for either version.

When consistent splitting holds, the basis elements $W_j^\pm$ span the manifolds of solutions decaying as $x \to +\infty$ (resp. $x \to -\infty$), and so vanishing of $D$ is associated with existence of an exponentially decaying eigenfunction and roots $\lambda$ correspond to standard eigenvalues. When extended consistent splitting holds but consistent splitting does not, then some of the basis elements may be nondecaying or even growing at infinity, and so roots correspond rather to "resonant poles". See [PW2] for further discussion. Thus, as mentioned before, our definition of point spectrum is in a generalized sense including all roots (including resonant poles) of the Evans function as defined in Definition 3.5. However, notice that if one has stable essential spectrum and unstable point (Evans) spectrum, then the unstable Evans spectra lies in the region of consistent splitting (excepting the degenerate case $\lambda = 0$) and hence corresponds to a spectral instability to localized perturbations. In particular, in this case is is possible to conclude nonlinear instability of the solitary wave by arguments like that of [Z8, Z9]. On the other hand, if one has both unstable essential and unstable point (Evans) spectrum, then the nature of the instability depends on which component of the spectra has larger real part; if the unstable point spectrum has larger maximum real part, then again this corresponds to an unstable localized eigenvalue, while if the essential spectrum has larger maximum real part, then we are essentially in the convective instability case briefly discussed in the introduction. The latter, convective, instability will be discussed further in Section 6.

## 3.3 The stability index

Next, we use the Evans function to seek conditions implying the existence of unstable point (Evans) spectrum. First, however, we need the following lemma which guarantees that our construction of the Evans function in the previous section is valid along the positive real axis.

**Lemma 3.8.** *Let $\tau_0$ be an equilibrium solution of the profile ODE* (2.4)*. Then, the open positive real axis is contained in the set of consistent splitting for the linearized St. Venant equations* (3.1) *if and only if $cdf_*(\tau_0) \le c^2$ or $c^2 - c_s^2 \le 0$. In any case, there exists a neighborhood of the origin which lies in the region of extended consistent splitting.*

**Remark 3.9.** *Notice that by Remark 2.4, the condition $c(df_*(\tau_0) - c) < 0$ is equivalent to the equilibrium $\tau_0$ being a saddle point of the profile ODE (2.4). It follows that, given any homoclinic solution of (2.4), the set $(0, \infty)$ is contained in the set of consistent splitting and hence any positive root of the Evans function corresponds to a spectral instability of the underlying wave to localized perturbations.*

*Proof.* Recall that the rightmost boundary of the essential spectrum is precisely the boundary of the region of consistent splitting. Thus, to establish the first claim it is sufficient to prove that the essential spectrum does not intersect the positive real axis if and only if $cdf_*(\tau_0) \leq c^2$ or $c^2 - c_s^2 \leq 0$.

This in turn follows by the Fourier analysis of Section 2.2. From (2.9) we see that the essential spectrum $\lambda = \lambda(k)$ intersects the real axis if and only if

$$-2ck\lambda + k\left(\frac{s+1}{\tau_0} - \frac{cr}{u_0} - \frac{c\nu k^2}{\tau_0^2}\right) = 0.$$

When $k \neq 0$ such roots must satisfy

$$\lambda = \frac{1}{2c}\left(\frac{s+1}{\tau_0} - \frac{cr}{u_0} - \frac{c\nu k^2}{\tau_0^2}\right) \tag{3.6}$$

and hence a sufficient condition that $\lambda \leq 0$ is that

$$\frac{s+1}{c\tau_0} \leq \frac{r}{u_0}.$$

Rearranging using the fact that $u_0 = \tau_0^{-(s+1)/r}$, we find that this last condition is equivalent to $\frac{1}{c}df_*(\tau_0) \leq 1$, which is equivalent to $c(df_*(\tau_0) - c) \leq 0$. Therefore, under this sign condition, we conclude that the only real roots $\lambda$ of (2.9) that can occur when $k \neq 0$ must be negative. But, when $k = 0$ we have the explicit roots $\lambda = 0$ and $\lambda = \frac{-r}{u_0}$, which are also non-negative and hence yields the desired contradiction.

Likewise, for $k \neq 0$, substituting (3.6) into the real part of the dispersion relation 2.9 yields the relation

$$\frac{\lambda}{2}\left(\frac{s+1}{c\tau_0} + \frac{r}{u_0} + \frac{\nu k^2}{\tau_0^2}\right) = k^2(c^2 - c_s^2),$$

which is a contradiction if $\lambda > 0$ and $c(df_*(\tau_0) - c) > 0$ and $c^2 - c_s^2 \leq 0$. Thus, we also see that the open positive real axis lies in the region of consistent splitting whenever $c^2 - c_s^2 \leq 0$.

If, on the other hand, $c(df_*(\tau_0) - c) > 0$ and $c^2 - c_s^2 > 0$, then, necessarily $|df_*| > |c_s|$, hence the subcharacteristic condition is violated and there exist essential spectra with strictly real part. Fixing $\tau_0$, hence $df_*$ and $c_s$, now vary the wave speed $c$. For $c = c_s$, we have as already noted the Hopf configuration shown in Figure 1 of a triple degeneracy with three distinct roots $k = 0, \pm k_*$ at $\lambda = 0$, and (by the sufficient condition already established), the positive real axis is contained in the region of consistent splitting. Recalling that changes in the wave speed $c$ by an amount $\Delta c$ corresponds to a translation in the roots of the dispersion

relation along the imaginary axis by an amount proportional to $i(\Delta c)k$, we find that for $c^2 \gtrless c_s^2$, the triple singularity breaks up into three distinct crossings of the imaginary axis, one at $\lambda = 0$ and two at $\pm ik_*(c - c_s)$. For $c^2 < c_s^2$, we have already shown that the real axis remains in the region of consistent splitting. See Figure 7(e),which shows an example of the essential spectrum in a case when $c > df_*(\tau_0) > c_s > 0$. When $c(df_*(\tau_0) - c) > 0$ and $c^2 > c_s^2$, therefore, the roots move in the opposite direction along the real axis, and the essential spectrum must intersect the positive real axis as in Figure 2. (Alternatively, we may see this by expansion of the dispersion relation in the vicinity of $\lambda = 0$ and $c = c_s$.) This verifies the first claim.

Finally, notice that expanding the dispersion relation (2.9) with the substitution $\mu = ik$, it follows that the matrix $A(x; 0) \equiv A_0(0)$ from the Evans system about the equilibrium solution $(\tau_0, u_0)$ with $\lambda = 0$ possess a one-dimensional center subspace. As the spectral gap between the stable and unstable subspaces of $A_0(0)$ persists under small perturbation, it follows that the corresponding matrices $A_0(\lambda)$ satisfy extended consistent splitting for $|\lambda|$ sufficiently small, which verifies the final claim. □

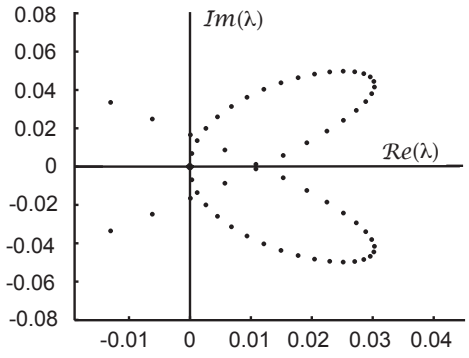


Figure 2: A numerical sampling of the (continuous) essential spectrum for the constant state $\tau_0 \approx 1.08507$ for the common case $(r, s) = (2, 0)$ when $c = 0.53$, $q \approx 1.53509$, $\nu = 0.1$, and $F = 6$. In particular, it is easily seen that $c(df_*(\tau_0) - c) > 0$ and $c^2 > c_s^2 \approx (0.361)^2$ in this case. Notice that the essential spectrum intersects the positive real axis, yielding an essential instability, but that the spectral curve does not exhibit the triple degeneracy at $\lambda = 0$ seen in Figure 1.

Following [GZ] then, we can analyze the Evans function on a set of the form $(-\varepsilon, \infty)$ for some $\varepsilon > 0$. In particular, by comparing high and low (real) frequency behavior of the Evans function, may compute a mod-two stability index giving partial stability information[8] in terms of geometric properties of the flow of the traveling-wave ODE: specifically, the sign

[8]This information is only partial in the sense that, while negativity of this mod-two index is sufficient for the existence of unstable real eigenvalues, its non-negativeness cannot be used to prove stability.

of a Melnikov derivative with respect to wave speed. To this end, we begin by analyzing the high (real) frequency asymptotics of the Evans function.

**Lemma 3.10.** $\mathrm{sgn}D(\lambda) \to 1$ *as* $\lambda \to +\infty$ *for* $\lambda$ *real.*

*Proof.* This may be checked by homotopy to an easy case, followed by direct computation. Or, we may observe that asymptotic behavior is determined by the principal part

$$\begin{pmatrix} \frac{\lambda}{c} & 0 & 0 \\ 0 & 0 & \bar{\tau}^2 \\ * & \frac{\lambda}{\nu} & 0 \end{pmatrix}$$

of $A(x,\lambda)$, hence by the Tracking Lemma of [GZ, ZH, MaZ3], $\det(W_1^-, W_2^-, W_3^+)_{x=0}$ is asymptotic to a positive multiple of $\det(V_1^-, V_2^-, V_3^+)$, which again is positive. See the computations of Section 4 for details of this decomposition into a principle part plus an asymptotically negligible part. □

In order to derive an instability index, we compare the above high frequency behavior with the low-frequency behavior near $\lambda = 0$. First, notice that differentiating (2.3) with respect to $x$ implies that $U_x$ satisfies the linearized eigenvalue equations (3.1) with $\lambda = 0$ and hence $D(0) = 0$. It follows negativity of $D'(0)$ is sufficient for the existence of a real, positive, unstable element of the point (Evans) spectrum of (3.1). Notice, however, that $D'(0) < 0$ always implies either the existence of an unstable localized eigenvalue (if this point lies in the region of consistent splitting), or else the presence of essential spectrum on the positive real axis. Therefore, given that $D'(0) < 0$ a conclusion can always be made concerning the stability of the underlying solitary wave: a time-exponential instability to localized perturbations or else a convective-time-oscillatory instability (as described in the introduction and in Section 6 below). It turns out that the sign of this derivative is intimately related to the underlying geometry of the ODE flow induced by the profile ODE. Indeed, for values of $(c,q)$ such that there is a smooth saddle equilibrium at $(\tau_0(c,q),0)$ in the traveling wave ODE, let $\bar{U}^+(c,q;x)$ parameterize the stable manifold at $(\tau_0,0)$ and $\bar{U}^-(c,q;x)$ the unstable manifold. Define the *Melnikov separation function*

$$d(c,q) = \det \begin{pmatrix} \bar{\tau}_x & \bar{\tau}^+ - \bar{\tau}^- \\ (\bar{\tau}_x)' & (\bar{\tau}^+ - \bar{\tau}^-)' \end{pmatrix} |_{x=0}, \tag{3.7}$$

and notice that this represents a signed distance of $\bar{U}^-$ from $\bar{U}^+$ along a normal section at $\bar{U}|_{x=0}$ oriented in the direction of $\bar{U}_x^\perp|_{x=0}$ with respect to the right hand rule; see Figure 3. As seen in the next lemma, the sign of the quantity $D'(0)$ is determined precisely by whether $d(c,q)$ is an increasing or decreasing function of the wave speed $c$. Notice that while this result is expected, the associated computations must still be carried out case by case. Furthermore, the structure of the proof for the rescaled Evans function (3.5) seems interesting in its own right.

**Lemma 3.11.** *If* $d(c,q) = 0$*, then for the linearized St. Venant eigenvalue equations* (3.1) *about the corresponding homoclinic orbit of* (2.4) *we have* $\mathrm{sgn}D'(0) = -\mathrm{sgn}\partial_c d(c,q)$.

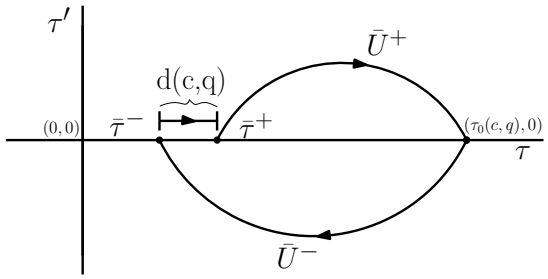


Figure 3: Depiction of the geometric interpretation of the Melnikov separation function $d(c,q)$, in the special case where $\bar{U}_x(0) = (0,1)^T$. By direct calculation, $d(c,q) < 0$.

*Proof.* This follows by a computation similar to those of [GZ, Z2, Go]. First, notice that since $\lambda = 0$ is a simple translational eigenvalue, we have $D(0) = 0$ and we may take without loss of generality $W_1^- = W_3^+ = \bar{U}'$ at $\lambda = 0$. Furthermore, a matrix perturbation argument at $\lambda = 0$ shows the unstable subspace of the asymptotic matrix $A_0(\lambda)$ can be analytically extended to a neighborhood of the origin, with limiting values at $\lambda = 0$ given by the direct sum of the unstable subspace of $A_0(0)$ and the vector $\left(1, -g_\tau(u_0,\tau_0)g_u(u_0,\tau_0)^{-1}, 0\right)^T$, with $g$ as in (2.6) It follows then that we can choose the vector $W_2^-(\cdot,0)$ to be asymptotically constant with

$$V_2^- = \lim_{x\to-\infty} W_2^-(x,0) = \left(1, \frac{-(s+1)u_0}{r\tau_0}, 0\right)^T = (1, -df_*(\tau_0), 0)^T,$$

where the last equality follows from the relation $\tau_0^{s+1}u_0^r = 1$. Moreover, assuming the homoclinic connection goes clockwise in the $(\tau,\tau')$ variables and that $\mu_+ < 0$ and $\mu_- > 0$ denote the decaying modes of the asymptotic matrix $A_0(0)$ at $\pm\infty$, respectively, we have

$$\begin{aligned} V_1^-(0) &= \left(-\tau_0, c\tau_0, c\mu_-\tau_0^{-1}\right)^T, \\ V_3^+(0) &= \left(\tau_0, -c\tau_0, -c\mu_+\tau_0^{-1}\right)^T, \end{aligned}$$

where we have used the fact that $u = -c\tau$ for the vectors $W_1^-(\cdot,0)$ and $W_3^+(\cdot,0)$. Therefore,

$$\begin{aligned} \det(V_1^-, V_2^+, V_3^+)|_{\lambda=0} &= \det\begin{pmatrix} -\tau_0 & 1 & \tau_0 \\ c\tau_0 & -df_*(\tau_0) & -c\tau_0 \\ c\mu_-\tau_0^{-1} & 0 & -c\mu_+\tau_0^{-1} \end{pmatrix} \\ &= c(\mu_- - \mu_+)\det\begin{pmatrix} -1 & 1 \\ c & -df_*(\tau_0) \end{pmatrix} \\ &= c(\mu_- - \mu_+)\left(df_*(\tau_0) - c\right). \end{aligned} \tag{3.8}$$

which is non-zero by assumption.

Continuing, since $\det(V_1^-, V_2^-, V_3^+)$ is non-vanishing and $\det(W_1^-, W_2^-, W_3^+)|_{x=0,\lambda=0} = 0$ we have

$$D'(0) = \frac{\partial_\lambda \det(W_1^-, W_2^-, W_3^+)|_{x=0}}{\det(V_1^-, V_2^-, V_3^+)}|_{\lambda=0}$$

and hence, to complete the proof then, we must calculate the numerator. Using the Leibnitz rule, we immediately find that

(3.9)
$$\begin{aligned}\partial_\lambda \det(W_1^-, W_2^-, W_3^+)|_{\lambda=0} &= \det(\partial_\lambda W_1^-, W_2^-, W_3^+)|_{\lambda=0} + \cdots + \det(W_1^-, W_2^-, \partial_\lambda W_3^+)|_{\lambda=0} \\ &= \det(\bar{U}_x, W_2^-, \partial_\lambda W_3^+ - \partial_\lambda W_1^-)|_{\lambda=0},\end{aligned}$$

where the vectors $\partial_\lambda W_j|_{\lambda=0}$ satisfy at

$$\partial_\lambda W_j'|_{\lambda=0} = A(x,0)\partial_\lambda W_j|_{\lambda=0} + \bar{U}' \tag{3.10}$$

for $j = 1, 3$. Furthermore, differentiating the stable and unstable manifold solutions of the traveling-wave ODE at the endstate $(\tau_0, u_0)$ (chosen in equilibrium) with respect to the wave speed $c$, we find

$$\partial_\lambda W_1^-|_{\lambda=0} = -\begin{pmatrix} \partial_c \bar{\tau}^- \\ \partial_c \bar{u}^- \\ \bar{\tau}^{-2}\partial_c \bar{u}^- \end{pmatrix}, \quad \partial_\lambda W_3^+|_{\lambda=0} = -\begin{pmatrix} \partial_c \bar{\tau}^+ \\ \partial_c \bar{u}^+ \\ \bar{\tau}^{-2}\partial_c \bar{u}^+ \end{pmatrix}.$$

Note this is a reflection of the similar role of $c$ and $-\lambda$ in the structure of the linearized traveling wave equation and in the linearized eigenvalue equation, respectively.

Next, setting $\lambda = 0$ in (3.1) and integrating from $x = -\infty$ to $x = 0$ implies

$$(u + c\tau)|_{x=0} = c - df_*(\tau_0)$$

for $(\tau, u) = ((W_2^-)_1, (W_2^-)_2)$, the first two components of the vector $W_2^-(\cdot, 0)$. Similarly, recalling (3.10) it follows that

$$(u + c\tau)|_{x=0} = \int_{\pm\infty}^{0} (\bar{u}_x + c\bar{\tau}_x)\, dx = (\bar{u} + c\bar{\tau})\,|_{x=\pm\infty}^{0}$$

for $(\tau, u) = (\bar{\tau}^\pm, \bar{u}^\pm)$. Therefore, returning to (3.9), we find that adding $\frac{1}{c}$ times the second row to the first yields

(3.11)
$$\begin{aligned}\partial_\lambda \det(W_1^-, W_2^-, W_3^+)|_{x=0,\lambda=0} &= \begin{pmatrix} 0 & \frac{1}{c}\,(c - df_*(\tau_0)) & 0 \\ \bar{u}_x & * & \partial_c(\bar{u}^- - \bar{u}^+) \\ \bar{\tau}^{-2}(\bar{u}_x)' & * & \bar{\tau}^{-2}\partial_c(\bar{u}^- - \bar{u}^+)' \end{pmatrix}|_{x=0} \\ &= \frac{1}{c}\,(df_*(\tau_0) - c)\det\begin{pmatrix} \bar{u}_x & \partial_c(\bar{u}^- - \bar{u}^+) \\ \bar{\tau}^{-2}(\bar{u}_x)' & \bar{\tau}^{-2}\partial_c(\bar{u}^- - \bar{u}^+)' \end{pmatrix}|_{x=0} \\ &= -c\bar{\tau}^{-2}(0)(df_*(\tau_0) - c)\det\begin{pmatrix} \bar{\tau}_x & \partial_c(\bar{\tau}^+ - \bar{\tau}^-) \\ (\bar{\tau}_x)' & \partial_c(\bar{\tau}^+ - \bar{\tau}^-)' \end{pmatrix}|_{x=0} \\ &= -c\bar{\tau}^{-2}(0)(df_*(\tau_0) - c)\partial_c d(c, q).\end{aligned}$$

The proof is now complete by dividing (3.11) by (3.8) and noting that $(\mu_- - \mu_+) > 0$. □

**Corollary 3.12.** $\mathrm{sgn}\partial_c d(c,q) < 0$ *is necessary for stability of point spectrum of the corresponding homoclinic, corresponding to an even number of roots with positive real part.*

**Remark 3.13.** In the stable case considered in [N2], for which periodic orbits appear as $c$ is decreased from the homoclinic speed $c_{\mathrm{hom}}$, we see that periodic orbits exist in the situation that $d < 0$, which should be visible from the phase portrait. That is, the lower orbit coming from the saddle point should pass *outside* the upper branch. Likewise, we can check the sign for Jin–Xin by looking at the phase portrait for nearby periodic case. In fact, we can compute directly that $\partial_c d > 0$ for the Jin–Xin case, as done in Section 3.4 below, yielding instability for that model.

**Remark 3.14.** Note that $\partial_c d < 0$ implies for $c < c_{\mathrm{hom}}$, where $c_{\mathrm{hom}}$ denotes the homoclinic wavespeed, that the unstable manifold at the saddle equilibrium spirals inward, either toward an attracting equilibrium in which case periodic orbits don't exist, or toward an attracting periodic cycle, in which case the enclosed equilibrium is a repeller. Likewise, $\partial_c d > 0$ implies for $c < c_{\mathrm{hom}}$ that the stable manifold at the saddle equilibrium spirals inward in backward $x$ either toward a repelling equilibrium in which case periodic orbits don't exist, or toward a repelling periodic cycle, in which case the enclosed equilibrium is an attractor in forward $x$. That is, generically, the stability condition $\partial_c d < 0$ is associated with the property that the enclosed equilibrium be a *repeller*, so long as decrease in speed from $c_{\mathrm{hom}}$ is associated with existence of periodic orbits. (If, rather, increase in speed is associated with existence of periodic orbits, then we reach the reverse conclusion that Evans stability corresponds to the property that the enclosed equilibrium be an attractor.) By Remark 2.4, therefore, we expect stability (of point spectra) of homoclinics in the St. Venant case studied in [N2].

As described in Remark 3.14, it is a curious fact that stability in temporal variable $t$ of the homoclinic as a solution of PDE (2.2) is associated with stability in spatial variable $x$ of nearby periodic orbits as solutions of the traveling-wave ODE (2.4), and, thereby,[9] instability of the equilibrium contained within the periodic orbits. The latter is also the condition that the homoclinic itself be stable in forward $x$-evolution as a solution of the traveling-wave ODE. It is not clear whether this is a coincidence, or plays a deeper role as a mechanism for stability. However, once we understand the existence theory (itself nontrivial, but often observed numerically), we may make conclusions readily about stability just by examining stability or instability of the enclosed equilibrium as a solution of the traveling-wave ODE.

## 3.4 The viscous Jin-Xin equations

While of theoretical interest, unfortunately the stability index $\partial_c d$ derived above appears to be analytically incomputable for the general St. Venant equations considered here (although, one can use the "rule of thumb" described in Remark 3.14 and the paragraph

[9] Assuming the generic case where there is only one limit cycle generated from increasing or decreasing the wave speed $c$, with an associated return map that is strictly attracting or strictly repelling.

immediately following). Next, we consider as simpler related example the viscous Jin–Xin model

$$\begin{aligned} \tau_t - u_x &= 0, \\ u_t - c_s^2 \tau_x &= -f(\tau) - u + u_{xx} \end{aligned} \tag{3.12}$$

for which we can directly calculate the value of $\partial_c d$. As we will see, Lemma 3.12 holds in this simpler setting as well. Considering traveling waves in the moving coordinate frame $x - ct$ gives traveling-wave ODE

$$(c^2 - c_s^2)\tau' = -f(\tau) + c\tau - q - c\tau'',$$

where $u = q - c\tau$. Taking $c = c_s$, this equation is seen to be Hamiltonian and reduces to the nonlinear oscillator

$$c\tau'' = -f(\tau) + c\tau - q, \tag{3.13}$$

for which all periodic orbits and the bounding homoclinic arise at once. Indeed, this equation may be integrated via quadrature: multiplying by $\tau'$ and integrating, we obtain

$$(c/2)(\tau')^2 = -F(\tau) + c\tau^2/2 - q\tau + H, \tag{3.14}$$

$F := \int f$, which is of standard Hamiltonian form with ODE energy $H$ and effective potential energy $V(\tau; c, q) = F(\tau) - \frac{c}{2}\tau^2 + q\tau$. In particular, we see that the homoclinic wavespeed $c_{hom}$ is precisely $c_s$ given in (3.12).

Denoting the roots of the equation $V'(\tau) = 0$ as $\tau_j$, we have that orbits through the equilibrium solutions $(\tau_j, 0)$ of (3.14) line on the level sets $V(\tau) = H$, and correspond to homoclinic orbits provided that $V''(\tau_j) < 0$. In this case, the orbits of (3.14) can be implicitly defined via the relation

$$\tau' = \pm\sqrt{(2/c)(-F(\tau) + c\tau^2/2 - q\tau + H)} \tag{3.15}$$

from which solutions of (3.12) may be obtained solving (3.15) for $\tau$ as a function of $x$ and using that $u = q - c\tau$. Furthermore, a direct calculation shows that the sign of $V''(\tau_j) = -df(\tau_j) + c$ alternates as $\tau_j$ increases, and hence we find that the subcharacteristic condition is satisfied if and only if $V''(\tau_j) < 0$. It follows that all non-trivial solitary wave solutions of (3.12) are stable to low-frequency perturbations, and hence have stable essential spectrum.

The analysis of the point spectrum of the corresponding homoclinic orbits is handled by the usual Evans function framework as described in Section 3.2. To this end, notice that in co-moving coordinates the linearized equations are

$$\begin{aligned} \tau_t - c\tau_x - u_x &= 0, \\ u_t - cu_x - c_s^2 \tau_x &= -df(\bar{\tau})\tau - u + u_{xx}, \end{aligned} \tag{3.16}$$

where $\bar{U} = (\bar{\tau}, \bar{u})$ denotes background profile. Taking the Laplace transform in time immediately leads to the linearized eigenvalue ODE

$$\begin{aligned} \lambda\tau - c\tau' - u' &= 0, \\ \lambda u - cu' - c_s^2\tau' &= -df(\bar{\tau})\tau - u + u'', \end{aligned} \tag{3.17}$$

governing the spectral stability of the underlying wave to localized perturbations. In order to use the abstract Evans function setup of Section 3.2, we write the eigenvalue system (3.17) as a first-order system of the form $W' = A(x, \lambda)W$, where

$$W := \begin{pmatrix} \tau \\ u \\ u' \end{pmatrix}, \qquad A := \begin{pmatrix} \lambda/c & 0 & -1/c \\ 0 & 0 & 1 \\ -c_s^2\lambda/c + df(\bar{\tau}) & \lambda + 1 & c_s^2/c - c \end{pmatrix}. \tag{3.18}$$

In order to apply Lemma 3.4, and hence define the corresponding Evans function $D(\lambda)$ as in (3.5), we must verify that we have extended consistent splitting in this case.

To obtain consistent splitting in the homoclinic case, we must have stability of constant solutions at the endpoint $\tau = 0$ from which the homoclinic originates, which as noted earlier is equivalent to the subcharacteristic condition

$$df_*(\tau_j) < c_s,$$

where $f_*(\tau) := -u_*(\tau) = f(\tau)$ is determined by the value $u_*(\tau) = -f(u)$ at equilibrium, hence $df_*(\tau) = df(\tau)$. Thus, the subcharacteristic condition is $df(\tau) < c_s$, and so as discussed above it is satisfied at alternate roots. (Recall that, by our previous analysis, instability of the constant solution is necessary for Hopf bifurcation and thus for existence of a nonlinear center and bounding homoclinic.) With this setup, we see that Lemma 3.4 applies to the eigenvalue system corresponding to (3.17) and hence we may define the Evans function $D(\lambda)$ as in (3.5). Furthermore, a direct calculation shows that the proof of Corollary 3.12 carries over line by line to the viscous Jin–Xin case considered here. It follows then that we can determine the stability of the solitary wave by direct considerations of the Melnikov separation function $d(c, q)$ defined in (3.7). It turns out that due to the geometric nature of the function $d(c, q)$ the sign of the derivative $\partial_c d$ is trivial to compute at the homoclinic.

Indeed, note that for general $c$ the traveling-wave ODE is

$$c\tau'' = -f(\tau) + c\tau - q - (c^2 - c_s^2)\tau'. \tag{3.19}$$

It follows that $H' = -(c^2 - c_s^2)|\tau'|^2$, where $H$ is the the Hamiltonian defined as in (3.14), and hence, for $c > c_s$, the ODE flow decreases the Hamiltonian $H$. Noting that $H$ is minimized at the equilibrium enclosed by the Homoclinic, it follows that we must have $d > 0$ for $0 < c - c_s \ll 1$ and hence we conclude that $\partial_c d > 0$. By Corollary 3.12 then, we conclude that the solitary waves of (3.12) always have unstable point spectrum.

This example, although much simpler than the full St. Venant equations, illustrates the power of being able to relate the stability of the solitary wave as a solution of the governing

PDE to information about Melnikov separation function $d(c,q)$, an inherently geometric quantity encoding information about the ODE phase space. For the St. Venant equations, however, we must resort to numerics to study the point spectrum of the linearized operator. This analysis is carried out in the following two sections. As we will see, however, although we are not able to analytically compute the stability index $\mathrm{sgn}\partial_c d(c,q)$ in this general case, our numerical experiments are consistent with the rule of thumb relating the PDE stability to the stability of the enclosed equilibrium solution of the ODE.

# 4 High-frequency asymptotics

Our next goal is to carry out a numerical Evans study of the point spectrum for the linearized equations (3.1) for homoclinic orbits corresponding to various choices of the turbulent friction parameters $(r,s)$. Indeed, later we will see that a winding number argument allows us to numerically compute the number of roots of the Evans function contained in a given compact region of the complex plane. The goal of this section is thus to eliminate the possibility of arbitrarily large unstable eigenvalues, so as to reduce our computations to a compact domain in $\lambda$ [Br, BrZ, HLZ, HLyZ1, HLyZ2]. This can be done by a number of techniques, including energy estimates and high-frequency asymptotics. As energy estimates degrade with small viscosity, we opt to use the latter techniques, which is well adapted to the situation of multiple scales such as are involved in our examples [PZ, Z5].

## 4.1 Approximate block-diagonalization

To begin, we show that the coefficient matrix $A(x,\lambda)$ in the Evans system (3.2) can be written, for $|\lambda| \gg 1$, as a block diagonal matrix plus an asymptotically small term. We begin by expanding $W'(\cdot) = A(\cdot,\lambda)W(\cdot)$ as $A = B + R$, where

$$
\begin{aligned}
B &:= \begin{pmatrix} \frac{\lambda}{c} & 0 & 0 \\ 0 & 0 & \bar\tau^2 \\ \frac{-\bar\alpha\lambda}{c\nu} & \frac{\lambda}{\nu} & 0 \end{pmatrix}, \\
R &:= \begin{pmatrix} 0 & 0 & -\frac{\bar\tau^2}{c} \\ 0 & 0 & 0 \\ \frac{(s+1)\bar\tau^s(q-c\bar\tau)^r-\bar\alpha_x}{\nu} & \frac{r\bar\tau^{s+1}(q-c\bar\tau)^{r-1}}{\nu} & \frac{-c\bar\tau^2+\bar\alpha\bar\tau^2/c}{\nu} \end{pmatrix} =: \begin{pmatrix} 0 & 0 & k \\ 0 & 0 & 0 \\ l & m & n \end{pmatrix},
\end{aligned}
\tag{4.1}
$$

where $\bar\alpha$ and $\bar\alpha_x$ are defined in (3.3) and where $\tau''$ is then computed using equation (2.4). Since $R = O(1)$ as $|\lambda| \to \infty$, we expect that the behavior of the Evans system (3.2) is governed by the principle part $B(x,\lambda)$ for $\lambda$ sufficiently large. Notice, however, that it is not straightforward to characterize this due to the multiple spectral scales associated with the growth of the eigenvalues of $B$. Indeed, a straightforward computation shows that the eigenvalues of the principle matrix $B$ are given by $\frac{\lambda}{c}$ and $\pm\bar\tau\sqrt{\frac{\lambda}{\nu}}$, and hence the spectrum of $B$ has two principle growth rates: order $\lambda$ and order $\lambda^{1/2}$. In order to keep track of both

of these scales, one must make a number of careful transformations, which we now describe in detail.

First, we introduce the transformations

$$T := \begin{pmatrix} 1 & 0 & 0 \\ 0 & 1 & 0 \\ \theta & 0 & 1 \end{pmatrix}, \qquad T^{-1} = \begin{pmatrix} 1 & 0 & 0 \\ 0 & 1 & 0 \\ -\theta & 0 & 0 \end{pmatrix}, \tag{4.2}$$

where $\theta := -\frac{\bar{\alpha}}{\nu}$. Then we readily see that

$$T^{-1}BT = \begin{pmatrix} \frac{\lambda}{c} & 0 & 0 \\ \theta\bar{\tau}^2 & 0 & \bar{\tau}^2 \\ 0 & \frac{\lambda}{\nu} & 0 \end{pmatrix}, \qquad T^{-1}RT = \begin{pmatrix} k\theta & 0 & k \\ 0 & 0 & 0 \\ l + n\theta - k\theta^2 & m & n - k\theta \end{pmatrix} \tag{4.3}$$

and, defining

$$B_1 := T^{-1}BT - \begin{pmatrix} 0 & 0 & 0 \\ \bar{\tau}^2\theta & 0 & 0 \\ 0 & 0 & 0 \end{pmatrix} = \begin{pmatrix} \lambda/c & 0 & 0 \\ 0 & 0 & \bar{\tau}^2 \\ 0 & \frac{\lambda}{\nu} & 0 \end{pmatrix}, \qquad W := TW_1, \tag{4.4}$$

we have $W_1' = (B_1 + R_1)W_1$, where

$$\begin{aligned} R_1 &:= T^{-1}RT - T^{-1}T' + \begin{pmatrix} 0 & 0 & 0 \\ \bar{\tau}^2\theta & 0 & 0 \\ 0 & 0 & 0 \end{pmatrix} \\ &= \begin{pmatrix} k\theta & 0 & k \\ \bar{\tau}^2\theta & 0 & 0 \\ l + n\theta - k\theta^2 - \theta' & m & n - k\theta \end{pmatrix} =: \begin{pmatrix} k_1 & 0 & l_1 \\ m_1 & 0 & 0 \\ n_1 & o_1 & p_1 \end{pmatrix}. \end{aligned} \tag{4.5}$$

Now, define

$$T_1 := \begin{pmatrix} 1 & 0 & 0 \\ 0 & 1 & 0 \\ 0 & 0 & \mu\sqrt{\lambda} \end{pmatrix}, \qquad T_1^{-1} = \begin{pmatrix} 1 & 0 & 0 \\ 0 & 1 & 0 \\ 0 & 0 & (\mu\sqrt{\lambda})^{-1} \end{pmatrix}, \tag{4.6}$$

where $\mu = \frac{1}{\bar{\tau}\sqrt{\nu}}$ and notice that

$$T_1^{-1}B_1T_1 = \begin{pmatrix} \frac{\lambda}{c} & 0 & 0 \\ 0 & 0 & \sqrt{\lambda}\mu\bar{\tau}^2 \\ 0 & \sqrt{\lambda}\mu\bar{\tau}^2 & 0 \end{pmatrix}, \qquad T_1^{-1}R_1T_1 = \begin{pmatrix} k_1 & 0 & l_1\mu\sqrt{\lambda} \\ m_1 & 0 & 0 \\ \frac{n_1}{\mu\sqrt{\lambda}} & \frac{o_1}{\mu\sqrt{\lambda}} & p_1 \end{pmatrix}. \tag{4.7}$$

Setting $W_1 = T_1W_2$, we thus have $W_2' = (B_2 + R_2)W_2$, where

$$B_2 := \begin{pmatrix} \frac{\lambda}{c} & 0 & l_1\mu\sqrt{\lambda} \\ 0 & 0 & \sqrt{\lambda}\mu\bar{\tau}^2 \\ 0 & \sqrt{\lambda}\mu\bar{\tau}^2 & 0 \end{pmatrix} \tag{4.8}$$

and

$$R_2 := T_1^{-1}R_1T_1 - T_1^{-1}T_1' - \begin{pmatrix} 0 & 0 & l_1\mu\sqrt{\lambda} \\ 0 & 0 & 0 \\ 0 & 0 & 0 \end{pmatrix} = \begin{pmatrix} k_1 & 0 & 0 \\ m_1 & o_1 & 0 \\ \frac{n_1}{\sqrt{\lambda}\mu} & \frac{o_1}{\sqrt{\lambda}\mu} & p_2 \end{pmatrix}, \tag{4.9}$$

with $p_2 := p_1 - \frac{\mu'}{\mu} = p_1 + \frac{\bar{\tau}'}{\bar{\tau}}$.

Continuing, define

$$T_2 := \begin{pmatrix} 1 & 0 & 0 \\ 0 & 1 & -1 \\ 0 & 1 & 1 \end{pmatrix}, \qquad T_1^{-1} = \begin{pmatrix} 1 & 0 & 0 \\ 0 & \frac{1}{2} & \frac{1}{2} \\ 0 & -\frac{1}{2} & \frac{1}{2} \end{pmatrix} \tag{4.10}$$

and set $B_3 := T_2^{-1}B_2T_2$ and $W_2 := T_2W_3$. Then by a direct calculation we have

$$W_3' = (B_3 + R_3)W_3, \tag{4.11}$$

where

$$B_3 = \begin{pmatrix} \frac{\lambda}{c} & l_1\mu\sqrt{\lambda} & l_1\mu\sqrt{\lambda} \\ 0 & \sqrt{\lambda}\mu\bar{\tau}^2 & 0 \\ 0 & 0 & -\sqrt{\lambda}\mu\bar{\tau}^2 \end{pmatrix} = \begin{pmatrix} \frac{\lambda}{c} & -\frac{\bar{\tau}}{c}\sqrt{\frac{\lambda}{\nu}} & -\frac{\bar{\tau}}{c}\sqrt{\frac{\lambda}{\nu}} \\ 0 & \bar{\tau}\sqrt{\frac{\lambda}{\nu}} & 0 \\ 0 & 0 & -\bar{\tau}\sqrt{\frac{\lambda}{\nu}} \end{pmatrix} \tag{4.12}$$

and

$$\begin{aligned} R_3 &:= T_2^{-1}R_2T_2 - T_2^{-1}T_2' \\ &= \begin{pmatrix} k_1 & 0 & 0 \\ \frac{m_1+n_1/\sqrt{\lambda}\mu}{2} & \frac{p_2+o_1/\sqrt{\lambda}\mu}{2} & \frac{p_2-o_1/\sqrt{\lambda}\mu}{2} \\ \frac{-m_1+n_1/\sqrt{\lambda}\mu}{2} & \frac{p_2+o_1/\sqrt{\lambda}\mu}{2} & \frac{p_2-o_1/\sqrt{\lambda}\mu}{2} \end{pmatrix} =: \begin{pmatrix} k_3 & 0 & 0 \\ l_3 & m_3 & n_3 \\ o_3 & m_3 & n_3 \end{pmatrix}. \end{aligned} \tag{4.13}$$

Finally, we introduce the transformations

$$T_3 := \begin{pmatrix} 1 & \frac{\tilde{\theta}}{\sqrt{\lambda}} & \frac{\tilde{\theta}}{\sqrt{\lambda}} \\ 0 & 1 & 0 \\ 0 & 0 & 1 \end{pmatrix}, \quad T_3^{-1} = \begin{pmatrix} 1 & -\frac{\tilde{\theta}}{\sqrt{\lambda}} & -\frac{\tilde{\theta}}{\sqrt{\lambda}} \\ 0 & 1 & 0 \\ 0 & 0 & 1 \end{pmatrix}, \tag{4.14}$$

where $\tilde{\theta} = \frac{\bar{\tau}}{\sqrt{\nu}}$ and note that

$$T_3^{-1}B_3T_3 = \begin{pmatrix} \frac{\lambda}{c} & -\frac{\bar{\tau}^2}{\nu} & \frac{\bar{\tau}^2}{\nu} \\ 0 & \bar{\tau}\sqrt{\frac{\lambda}{\nu}} & 0 \\ 0 & 0 & -\bar{\tau}\sqrt{\frac{\lambda}{\nu}} \end{pmatrix},$$

$$T_3^{-1}R_3T_3 = \begin{pmatrix} k_3 - (l_3+o_3)\frac{\tilde{\theta}}{\sqrt{\lambda}} & (k_3 - 2m_3 - (l_3+o_3)\frac{\tilde{\theta}}{\sqrt{\lambda}})\frac{\tilde{\theta}}{\sqrt{\lambda}} & (k_3 - 2n_3 - (l_3+o_3)\frac{\tilde{\theta}}{\sqrt{\lambda}})\frac{\tilde{\theta}}{\sqrt{\lambda}} \\ l_3 & m_3 + l_3\frac{\tilde{\theta}}{\sqrt{\lambda}} & n_3 + l_3\frac{\tilde{\theta}}{\sqrt{\lambda}} \\ o_3 & m_3 + o_3\frac{\tilde{\theta}}{\sqrt{\lambda}} & n_3 + o_3\frac{\tilde{\theta}}{\sqrt{\lambda}} \end{pmatrix}. \tag{4.15}$$

Defining then

$$B_4 \;=\; \begin{pmatrix} \frac{\lambda}{c} & 0 & 0 \\ 0 & \bar{\tau}\sqrt{\frac{\lambda}{\nu}} & 0 \\ 0 & 0 & -\bar{\tau}\sqrt{\frac{\lambda}{\nu}} \end{pmatrix}, \tag{4.16}$$

and

$$R_4 \;=\; T_3^{-1} R_3 T_3 + \begin{pmatrix} 0 & -\frac{\bar{\tau}^2}{\nu} - \frac{\tilde{\theta}'}{\sqrt{\lambda}} & \frac{\bar{\tau}^2}{\nu} - \frac{\tilde{\theta}'}{\sqrt{\lambda}} \\ 0 & 0 & 0 \\ 0 & 0 & 0 \end{pmatrix}, \tag{4.17}$$

it follows that the original Evans system (3.2) can be written in the approximately block-diagonal system

$$W' = (B_4(x,\lambda) + R_4(x,\lambda))\, W \tag{4.18}$$

where $R_4 = o(\lambda^\varepsilon)$ as $\lambda \to \infty$ for all $\varepsilon > 0$. With this result in hand, we can now obtain bounds on the size of the unstable eigenvalues $\lambda$ corresponding to the linearized St. Venant equations (3.1). Before stating these bounds, however, we need the following abstract tracking lemma concerning the eigenspaces of approximately block-diagonal systems.

## 4.2 Quantitative tracking lemma

We now recall the following quantitative estimate [HLyZ1, HLyZ2]. Consider an asymptotically constant approximately block-diagonal system $W' = (M + \Theta)(x)W$,

$$W = \begin{pmatrix} W_- \\ W_+ \end{pmatrix}, \quad M = \begin{pmatrix} M_- & 0 \\ 0 & M_+ \end{pmatrix}, \quad \Theta = \begin{pmatrix} \Theta_{--} & \Theta_{-+} \\ \Theta_{+-} & \Theta_{++} \end{pmatrix}, \tag{4.19}$$

with $\Re M_- \leq c_- I$ and $\Re M_+ \geq c_+ I$ satisfying

$$c_+ - c_- \geq \delta(x) > 0, \tag{4.20}$$

where $\Re M := (1/2)(M + M^*)$ denotes the symmetric part of a matrix $M$.

Denote by

$$\zeta_\pm(x) := \frac{\delta - |\Theta_{--}| - |\Theta_{++}|}{2|\Theta_{+-}|} \pm \sqrt{\Big(\frac{\delta - |\Theta_{--}| - |\Theta_{++}|}{2|\Theta_{+-}|}\Big)^2 - \frac{|\Theta_{-+}|}{|\Theta_{+-}|}} \tag{4.21}$$

the roots of

$$P(\delta, x) := \Big( -\delta + |\Theta_{--}| + |\Theta_{++}|\Big)\zeta + |\Theta_{-+}| + |\Theta_{+-}|\zeta^2 = 0, \tag{4.22}$$

where, here and below, $|\cdot|$ denotes the $\ell^2$ matrix operator norm.

**Lemma 4.1** ([HLyZ1, HLyZ2])**.** *Suppose that*

$$\delta > |\Theta_{--}| + |\Theta_{++}| + 2\sqrt{|\Theta_{-+}||\Theta_{+-}|}. \tag{4.23}$$

*Then, (i)* $0 < \zeta_- < \zeta_+$*, (ii) the invariant subspaces of the limiting coefficient matrices* $(M + \Theta)(\pm\infty)$ *are contained in distinct cones*

$$\Omega_- = \{|W_-|/|W_+| \leq \zeta_-\}, \quad \Omega_+ = \{|W_-|/|W_+| \geq \zeta_+\},$$

*and (iii) denoting by* $S^+$ *the total eigenspace of* $(M + \Theta)(+\infty)$ *contained in* $\Omega_+(+\infty)$ *and* $U^-$ *the total eigenspace of* $(M + \Theta)(-\infty)$ *contained in* $\Omega_-(-\infty)$*, the manifolds of solutions of* (4.19) *asymptotic to* $S^+$ *at* $x = +\infty$ $U^-$ *at* $x = -\infty$ *are separated for all* $x$*, lying in* $\Omega_+$ *and* $\Omega_-$ *respectively. In particular, there exist no solutions of* (4.19) *asymptotic to* $S^+$ *at* $+\infty$ *and to* $U^-$ *at* $-\infty$*.*

**Remark 4.2.** In the case that $c_- < 0$ at $+\infty$ and $c_+ > 0$ at $x = -\infty$, $S^+$ and $U^-$ correspond to the stable subspace at $+\infty$ and the unstable subspace at $-\infty$ of the limiting constant-coefficient matrices, and we may conclude nonexistence of decaying solutions of (4.19), or nonvanishing of the associated Evans function. More generally, even if (as here), the property of decay is lost as we traverse the boundary of consistent splitting, so long as there remains a positive spectral gap $\delta$, and (4.23) remains satisfied, we may still conclude nonvanishing of the Evans function defined as above by continuous extension of subspaces $U^-$ and $S^+$.

*Proof.* ([HLyZ1, HLyZ2]) From (4.19), we obtain readily

$$\begin{aligned} |W_-|' &\leq c_-|W_-| + |\Theta_{--}||W_-| + |\Theta_{-+}||W_+|, \\ |W_+|' &\geq c_+|W_+| - |\Theta_{+-}||W_-| - |\Theta_{++}||W_+|, \end{aligned} \tag{4.24}$$

from which, defining $\zeta := |W_-|/|W_+|$, we obtain by a straightforward computation the Riccati equation $\zeta' \leq P(\zeta, x)$.

Consulting (4.22), we see that $\zeta' < 0$ on the interval $\zeta_- < \zeta < \zeta_+$, whence $\Omega_- := \{\zeta \leq \zeta_-\}$ is an invariant region under the forward flow of (4.19); moreover, this region is exponentially attracting for $\zeta < \zeta_+$. A symmetric argument yields that $\Omega_+ := \{\zeta \geq \zeta_+\}$ is invariant under the backward flow of (4.19), and exponentially attracting for $\zeta > \zeta_-$. Specializing these observations to the constant-coefficient limiting systems at $x = -\infty$ and $x = +\infty$, we find that the invariant subspaces of the limiting coefficient matrices must lie in $\Omega_-$ or $\Omega_+$. (This is immediate in the diagonalizable case; the general case follows by a limiting argument.)

By forward (resp. backward) invariance of $\Omega_-$ (resp. $\Omega_+$), under the full, variable-coefficient flow, we thus find that the manifold of solutions initiated along $U^+$ at $x = -\infty$ lies for all $x$ in $\Omega_+$ while the manifold of solutions initiated in $S^+$ at $x = +\infty$ lies for all $x$ in $\Omega_-$. Since $\Omega_-$ and $\Omega_+$ are distinct, we may conclude that under condition (4.23) there are no solutions asymptotic to both $U^-$ and $S^+$. □

### 4.3 Bounds on unstable eigenvalues

With the above tracking lemma in hand, we are able to state our main result concerning the confinement of the unstable eigenvalues of (3.1). After a change of coordinates switching $-$ and $+$, using notations of Section 4.1, equation (4.18) determines a system of form (4.19) with

$$
\begin{aligned}
M_+ &= \begin{pmatrix} \frac{\lambda}{c} & 0 \\ 0 & \bar\tau\sqrt{\frac{\lambda}{\nu}} \end{pmatrix}, \quad M_- = \left(-\bar\tau\sqrt{\tfrac{\lambda}{\nu}}\right) \\
\Theta_{++} &= \Theta^0_{++} + \lambda^{-1/2}\Theta^1_{++} + \lambda^{-1}\Theta^2_{++} + \lambda^{-3/2}\Theta^3_{++} \\
&:= \begin{pmatrix} k_1 & -\frac{\bar\tau^2}{\nu} \\ \frac{m_1}{2} & \frac{p_2}{2} \end{pmatrix} + \lambda^{-1/2}\begin{pmatrix} 0 & -\tilde\theta' + \tilde\theta(k_1 - p_2) \\ \frac{n_1}{2\mu} & \frac{o_1}{2\mu} - \tilde\theta\frac{m_1}{2} \end{pmatrix} \\
&\quad + \lambda^{-1}\begin{pmatrix} -\tilde\theta\frac{n_1}{\mu} & -\tilde\theta\frac{o_1}{\mu} \\ 0 & \tilde\theta\frac{n_1}{2\mu} \end{pmatrix} + \lambda^{-3/2}\begin{pmatrix} 0 & -\tilde\theta^2\frac{n_1}{\mu} \\ 0 & 0 \end{pmatrix},
\end{aligned}
\tag{4.25}
$$

$$
\begin{aligned}
\Theta_{+-} &= \Theta^0_{+-} + \lambda^{-1/2}\Theta^1_{+-} + \lambda^{-1}\Theta^2_{+-} + \lambda^{-3/2}\Theta^3_{+-} \\
&:= \begin{pmatrix} \frac{\bar\tau^2}{\nu} \\ \frac{p_2}{2} \end{pmatrix} + \lambda^{-1/2}\begin{pmatrix} -\tilde\theta' + \tilde\theta(k_1 - p_2) \\ -\frac{o_1}{2\mu} + \tilde\theta\frac{m_1}{2} \end{pmatrix} + \lambda^{-1}\begin{pmatrix} \tilde\theta\frac{o_1}{\mu} \\ \tilde\theta\frac{n_1}{2\mu} \end{pmatrix} + \lambda^{-3/2}\begin{pmatrix} -\tilde\theta^2\frac{n_1}{\mu} \\ 0 \end{pmatrix}, \\
\Theta_{-+} &= \Theta^0_{-+} + \lambda^{-1/2}\Theta^1_{-+} + \lambda^{-1}\Theta^2_{-+} \\
&:= \begin{pmatrix} -\frac{m_1}{2} & \frac{p_2}{2} \end{pmatrix} + \lambda^{-1/2}\begin{pmatrix} \frac{n_1}{2\mu} & \frac{o_1}{2\mu} - \tilde\theta\frac{m_1}{2} \end{pmatrix} + \lambda^{-1}\begin{pmatrix} 0 & \tilde\theta\frac{n_1}{2\mu} \end{pmatrix}, \\
\Theta_{--} &= \Theta^0_{--} + \lambda^{-1/2}\Theta^1_{--} + \lambda^{-1}\Theta^2_{--} \\
&:= \begin{pmatrix} \frac{p_2}{2} \end{pmatrix} + \lambda^{-1/2}\begin{pmatrix} -\frac{o_1}{2\mu} - \tilde\theta\frac{m_1}{2} \end{pmatrix} + \lambda^{-1}\begin{pmatrix} \tilde\theta\frac{n_1}{2\mu} \end{pmatrix},
\end{aligned}
$$

for which evidently $\delta \geq \bar\tau\Re\sqrt{\frac{\lambda}{\nu}} \geq |\lambda|^{1/2}\frac{\bar\tau}{\sqrt{2\nu}}$ when $\Re\lambda \geq 0$. Then a direct application of Lemma 4.1 yields the following high-frequency bound.

**Corollary 4.3.** *There are no unstable roots $\lambda$, with $\Re\lambda \geq 0$, of $D$ with $|\lambda| > \max_x R^4$, where $R$ is the only positive root of $X^8 - a_0X^6 - a_{1/2}X^5 - a_1X^4 - a_{3/2}X^3 - a_2X^2 - a_{5/4}X - a_3$*

*with*

$$
\begin{aligned}
a_0 &= \frac{\sqrt{2\nu}\left(|\Theta^0_{--}| + |\Theta^0_{++}| + 2\sqrt{|\Theta^0_{-+}||\Theta^0_{+-}|}\right)}{\bar\tau},\\
a_{1/2} &:= \frac{\sqrt{2\nu}2\sqrt{|\Theta^0_{-+}||\Theta^1_{+-}| + |\Theta^1_{-+}||\Theta^0_{+-}|}}{\bar\tau},\\
a_1 &:= \frac{\sqrt{2\nu}\left(|\Theta^1_{--}| + |\Theta^1_{++}| + 2\sqrt{|\Theta^1_{-+}||\Theta^1_{+-}| + |\Theta^0_{-+}||\Theta^2_{+-}| + |\Theta^2_{-+}||\Theta^0_{+-}|}\right)}{\bar\tau},\\
a_{3/2} &:= \frac{\sqrt{2\nu}2\sqrt{|\Theta^0_{-+}||\Theta^3_{+-}| + |\Theta^1_{-+}||\Theta^2_{+-}| + |\Theta^2_{-+}||\Theta^1_{+-}|}}{\bar\tau},\\
a_2 &:= \frac{\sqrt{2\nu}\left(|\Theta^2_{--}| + |\Theta^2_{++}| + 2\sqrt{|\Theta^2_{-+}||\Theta^2_{+-}| + |\Theta^1_{-+}||\Theta^3_{+-}|}\right)}{\bar\tau},\\
a_{5/4} &:= \frac{\sqrt{2\nu}2\sqrt{|\Theta^2_{-+}||\Theta^3_{+-}|}}{\bar\tau},\\
a_3 &:= \frac{\sqrt{2\nu}|\Theta^3_{++}|}{\bar\tau}.
\end{aligned}
\tag{4.26}
$$

*In particular there are no unstable roots $\lambda$ with modulus larger than $\tilde R^4$ where $\tilde R$ is the only positive root of $X^8 - (\max a_0)X^6 - (\max a_{1/2})X^5 - (\max a_1)X^4 - (\max a_{3/2})X^3 - (\max a_2)X^2 - (\max a_{5/4})X - \max a_3$.*

To aid in the utilization of the bounds in Corollary 4.3, note that $R^4$ is smaller than

- the square of the only positive root of
$$
\begin{aligned}
X^4 - \left(a_0X + \frac{a_{1/2}}{2}\right)X^3 - \left(\frac{a_{1/2}}{2} + a_1 + \frac{a_{3/2}}{2}\right)X^2 - \left(\frac{a_{3/2}}{2} + a_2 + \frac{a_{5/4}}{2}\right)X - \left(\frac{a_{5/4}}{2} + a_3\right)&\\
=: X^4 - \tilde a_0X^3 - \tilde a_1X^2 - \tilde a_2X - \tilde a_3;&
\end{aligned}
\tag{4.27}
$$

- the only positive root of
$$
X^2 - (\tilde a_0^2 + 2\tilde a_1 + \tilde a_2)X - (\tilde a_2 + 2\tilde a_3). \tag{4.28}
$$

Both bounds can be explicitly given. Here, however, we determine $R$ by numerical solution of the full eighth-order polynomial equation given in Corollary (4.3).

*Proof.* By Lemma 4.1, the triangle inequality and subadditivity of the square-root function,

there are no unstable eigenvalues $\lambda$ with

(4.29)

$$
\begin{aligned}
|\lambda|^{1/2} > & \frac{\sqrt{2\nu}\left(|\Theta^0_{--}| + |\Theta^0_{++}| + 2\sqrt{|\Theta^0_{-+}||\Theta^0_{+-}|}\right)}{\bar\tau} \\
& + |\lambda|^{-1/4}\frac{\sqrt{2\nu}2\sqrt{|\Theta^0_{-+}||\Theta^1_{+-}| + |\Theta^1_{-+}||\Theta^0_{+-}|}}{\bar\tau} \\
& + |\lambda|^{-1/2}\frac{\sqrt{2\nu}\left(|\Theta^1_{--}| + |\Theta^1_{++}| + 2\sqrt{|\Theta^1_{-+}||\Theta^1_{+-}| + |\Theta^0_{-+}||\Theta^2_{+-}| + |\Theta^2_{-+}||\Theta^0_{+-}|}\right)}{\bar\tau} \\
& + |\lambda|^{-3/4}\frac{\sqrt{2\nu}2\sqrt{|\Theta^0_{-+}||\Theta^3_{+-}| + |\Theta^1_{-+}||\Theta^2_{+-}| + |\Theta^2_{-+}||\Theta^1_{+-}|}}{\bar\tau} \\
& + |\lambda|^{-1}\frac{\sqrt{2\nu}\left(|\Theta^2_{--}| + |\Theta^2_{++}| + 2\sqrt{|\Theta^2_{-+}||\Theta^2_{+-}| + |\Theta^1_{-+}||\Theta^3_{+-}|}\right)}{\bar\tau} \\
& + |\lambda|^{-5/4}\frac{\sqrt{2\nu}2\sqrt{|\Theta^2_{-+}||\Theta^3_{+-}|}}{\bar\tau} \\
& + |\lambda|^{-3/2}\frac{\sqrt{2\nu}|\Theta^3_{++}|}{\bar\tau},
\end{aligned}
$$

also written $|\lambda|^{1/2} > a_0 + a_{1/2}|\lambda|^{-1/4} + a_1|\lambda|^{-1/2} + a_{3/2}|\lambda|^{-3/4} + a_2|\lambda|^{-1} + a_{5/4}|\lambda|^{-5/4} + a_3|\lambda|^{-3/2}$. The condition is satisfied as soon as $|\lambda|^{1/4} > \max_x R$. □

For those interested in reproducing or using the high frequency bounds obtained above, we record in the Appendix the formulas for the various terms listed above in terms of the original underlying homoclinic profile.

**Remark 4.4.** *By similar estimates (see the abstract Tracking Lemma of [MaZ3, PZ, Z5]), one may obtain as in [HLyZ1] the asymptotic description*

$$D(\lambda) \sim c_1 e^{c_2\sqrt{\lambda}} \tag{4.30}$$

*for some $c_1, c_2 \in \mathbb{R}$ as $|\lambda| \to \infty$, with convergence at rate $\mathcal{O}(|\lambda|^{-1/2})$.*

# 5 Numerical investigations

In this section, we carry out a numerical study of the stability of the solitary wave solutions of the generalized St. Venant equations. In particular, we perform numerical Evans function calculations to detect the presence of unstable point spectrum. In the two examples considered, we find that one has stable essential spectrum with unstable point spectrum, while the other has stable point spectrum with unstable essential spectrum. Furthermore, for the latter case we perform a time evolution study to illustrate the convective nature of

the instability arising from the essential spectrum. For illustrative purposes, however, we choose to perform a numerical Evans study of the solitary wave solutions of the viscous Jin–Xin equations. Recall that by our considerations in Section 3.4, we expect the linearization to have unstable point spectrum, in particular, a positive real eigenvalue, corresponding to exponential instability of the solitary wave.

## 5.1 Jin–Xin example

To begin, consider first the set of equations

$$\begin{aligned} &\tau_t - u_x = 0, \\ &u_t - \tau_x = \tau^{-1/2} - u + u_{xx}, \end{aligned} \tag{5.1}$$

corresponding to (3.12) with nonlinearity $f(\tau) = -\tau^{-1/2}$, mimicking the St. Venant structure, and $c_s = 1$. For this example, we consider the solitary wave profile $\bar{U} = (\bar{\tau}, \bar{u})$ satisfying the ODE

$$\frac{1}{2}\left(\bar{\tau}'\right)^2 = 2\bar{\tau}^{1/2} + \frac{1}{2}\bar{\tau}^2 - 2\bar{\tau} - \frac{1}{2}$$

corresponding to the profile ODE (3.14) with $(q, H) = \left(2, -\frac{1}{2}\right)$. This profile is numerically generated using MATLAB's RK45 solver ODE45 [KL] and is depicted in phase space in Figure 4(a) and is plotted against the spatial variable $x$ in Figure 4(b). To study the spectral stability of this profile, we must next consider the linearized eigenvalue equations (3.17) with $c_s = 1$ and $df(\bar{\tau}) = -\frac{1}{2}\bar{\tau}^{-3/2}$. Since we expect the existence of a real unstable eigenvalue by the calculations in Section 3.4, we numerically compute the Evans function along the positive real line and show the existence of a positive root. This is accomplished here by using the polar-coordinate method of [HuZ] as well as other standard procedures; see also [BrZ, Z6]. In particular, the Evans function was computed in MATLAB using RK45 to solve the associated ODE's. The adaptive error control provided by RK45 gives an estimate on truncation error which, by the results of [Z6], then translate to convergence error estimates. Furthermore, we find analytically varying initializing bases $\{R_j^{\pm}\}$ for the Evans function computation via the method of Kato; see [GZ, HuZ, BrZ, BHZ]. Following this procedure then, we plot in Figure 4 (c) the output as evaluated on the interval $[0, 1]$ and clearly see that $D(\lambda)$ vanishes (geometrically) twice within this interval: once at $\lambda = 0$ corresponding to the simple translational eigenvalue and once at a positive $\lambda_0 > 0$ yielding the expected instability.

An alternate way of numerically seeing this instability through the use of an Evans function is through the use of a winding number calculation. Indeed, the analyticity of the Evans function on the spectral parameter $\lambda$ implies the number of solutions of the equation $D(\lambda) = 0$ within the bounded component of a contour $\Gamma$, along which $D|_\Gamma$ is non-vanishing,

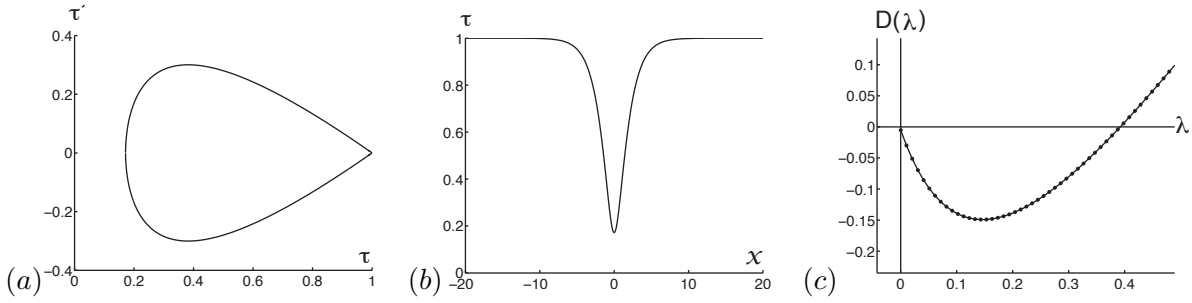


Figure 4: Evans function output for the Jin-Xin equations with $f(\tau) = -\tau^{-1/2}$ and $c_s = 1$, $q = 2$, and $H = -1/2$. We display the homoclinic profile in phase space ($\tau$ vs. $\tau'$) in Figure (a) and against the spatial variable ($\tau$ vs. $x$) in Figure (b). In Figure (c), we plot the Evans function output evaluated on the real line ($D(\lambda)$ vs. $\lambda \in \mathbb{R}$), illustrating the existence of an unstable positive eigenvalue.

can be calculated via the winding number[10]

$$\frac{1}{2\pi i}\int_\Gamma \frac{D'(\lambda)}{D(\lambda)}d\lambda. \tag{5.2}$$

Notice that unlike our Evans function calculations in Sections 3.3 and 3.4, which could only be used to yield a mod-two count of the real roots of $D(\lambda) = 0$ (hence also of all positive real part roots), this method allows one to exclude the possibility of unstable eigenvalues within a given compact domain. This advantage will be exploited below in conjunction with the eigenvalue bounds of Corollary 4.3 to conclude stability of the point spectrum for particular underlying periodic waves (that is, not only the absence of real unstable eigenvalues but of *any* unstable eigenvalues). To illustrate the numerical procedure, we consider again the Jin–Xin profile studied above. Notice that finding the analytically varying initializing bases $\{R_j^\pm\}$ as described above preserves analyticity of the Evans function allowing us to use, via the argument principle, a winding number computation to determine the presence of roots inside a given contour. For this example, we choose a semi-circular contour of radius one and inner circle radius $10^{-3}$. Notice that for a winding number calculation the contour must not go through the origin since $D(0) = 0$, and hence we must deform the standard semi-circular contour slightly near the origin. Using a sufficient number of mesh points then, we can ensure the relative change in $D(\lambda_j)$ between consecutive mesh points $\{\lambda_j\}$ is less than 0.2, thus assuring an accurate winding number count by Rouché's Theorem. For this specific example, a plot of the Evans function output restricted to the semi-circular contour described above is shown in Figure 5. From this, it is easily seen that the winding number about zero is one, again verifying the expected instability.

[10]Notice that the following integral simply calculates the net number of times the image of the curve $\Gamma$ under $D(\cdot)$ winds around the origin in the complex plane.

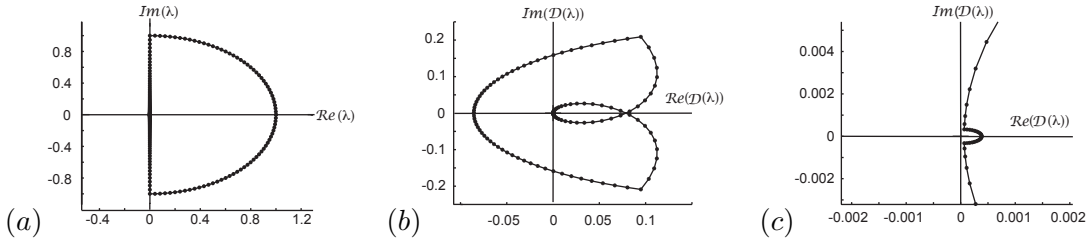


Figure 5: Evans function output for the Jin-Xin equations with $f(\tau) = -\tau^{-1/2}$ and $c_s = 1$, $q = 2$, and $H = -1/2$. Figure (a) depicts the semi-circular contour in the spectral plane used for the winding number calculation. In Figure (b), we have the Evans function output evaluated along the contour and in Figure (c) we zoom in on Figure (b) near the origin. In this case, the winding number about the origin of the curve in Figure (b) is one, implying the existence of an unstable eigenvalue within the open region in Figure (a) bounded by the semi-circular contour, as expected; see Figure 4(c).

## 5.2 St. Venant example

Next, we perform the analogous numerical study for the St. Venant equations (2.2) for two distinct values of the turbulent friction parameters. First, we consider the case $(r, s) = (1, 1)$ demonstrating stable essential spectrum and unstable point spectrum. Second, we consider the common case $(r, s) = (2, 0)$ demonstrating unstable essential spectrum and stable point spectrum. As mentioned in the introduction, this instability is convective in nature and we demonstrate this with a time evolution study.

### 5.2.1 Case $(r, s) = (1, 1)$

First, consider the equation

$$\begin{aligned} \tau_t - u_x &= 0, \\ u_t + ((0.444)^{-1}\tau^{-2})_x &= 1 - \tau^2 u + 20(\tau^{-2}u_x)_x, \end{aligned} \tag{5.3}$$

corresponding to the St. Venant system (2.2) with $(r, s) = (1, 1)$, $F = 0.222$, and $\nu = 20$. In this example, we consider the traveling wave profile associated with the corresponding traveling wave ODE (2.4) with wave speed $c \approx 3.1869$ and integration constant $q = 1 + c$. Following the protocol previously described, in Figure 6(a) we depict the corresponding orbit in phase space along with the Evans function output along the real line. From Figure 6(b), it is clear there exists an unstable real eigenvalue associated with this profile. Although not depicted here, this was further verified by a winding number calculation as in the Jin–Xin case above, in which one finds a winding number of one for an appropriate semicircular contour. Moreover, notice that the limiting constant state $(1, 0)$ satisfies the subcharacteristic condition

$$2\sqrt{F} < \left( \lim_{x \to \pm\infty} \tau(x) \right)^{3/2}$$

corresponding to spectral stability of the limiting state. It follows that although this profile admits unstable point spectrum, its essential spectrum is stable. We verify this numerically using the SpectrUW package developed at the University of Washington[DK], which is designed to find the essential spectrum of linear operators with periodic coefficients by using Fourier-Bloch decompositions and Galerkin truncation; see [CuD, CDKK, DK] for further information and for details concerning convergence. Although this package is designed for periodic problems, the essential spectrum corresponding to the limiting constant state (treated as a periodic function) of our homoclinic is precisely the essential spectrum of the original homoclinic profile, and hence we can numerically compute the essential spectrum of a solitary wave using SpectrUW in this way. In particular, we find that the essential spectrum is stable, as expected; see Figure 6(c).

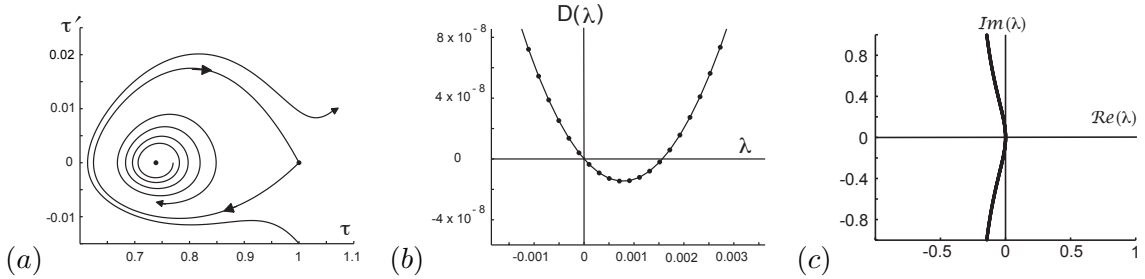


Figure 6: Demonstration of unstable point spectrum for the generalized St. Venant system. Here $r = s = 1$, $\nu = 20$, $F = 0.222$, $c \approx 3.1869$, and $q = 1 + c$. We have the phase portrait plotting $\tau$ verse $\tau'$ in Figure (a), and the Evans function evaluated along the real line ($D(\lambda)$ vs. $\lambda \in \mathbb{R}$) in Figure (b). Finally, Figure (c) depicts the numerical evaluation of the essential spectrum of the homoclinic using the SpectrUW package.

We now wish to connect this numerical experiment to the analytical Evans function calculations of Section 3.3, in particular Corollary 3.12 and Remark 3.14. To this end, we note that numerically it is found that periodic orbits exist for the system (5.3) as $c$ is increased through the homoclinic wave speed, which here we have chosen as $c_{\text{hom}} \approx 3.1869$. Furthermore, as seen by Figure 6(a) the equilibrium solution enclosed by the homoclinic orbit is a repeller. Together these considerations suggest that $\partial_c d(c, q) > 0$ by our discussion in Remark 3.14. This may be verified by noting from Figure 6(b) that $D'(0) < 0$ and using Lemma 3.11. Thus, the instability of this profile follows trivially from direct analysis of the corresponding phase portrait and Corollary 3.12. Notice, however, that this example shows the dependence of the "repeller/attractor" rule of thumb on how the periodic orbits are generated from the homoclinic.

### 5.2.2 Case $(r, s) = (2, 0)$

Next, we consider the equation

$$\begin{aligned} \tau_t - u_x &= 0, \\ u_t + ((18)^{-1}\tau^{-2})_x &= 1 - \tau u^2 + 0.1(\tau^{-2}u_x)_x, \end{aligned} \tag{5.4}$$

corresponding to the St. Venant system with $(r, s) = (2, 0)$, $F = 9$, and $\nu = 0.1$. Here, we consider the solitary wave profile associated with the corresponding profile ODE with wave speed $c \approx 0.7849$ and integration constant $q = 1 + c$, which is depicted in phase space in Figure 7(a). We begin by discussing the point spectrum associated to this solitary wave solution. Noting that periodic orbits are seen to be numerically generated as the wave speed is decreased from the homoclinic speed, the fact that the equilibrium enclosed in the homoclinic is a repeller suggests that $\partial_c d(c, q) < 0$ by Remark 3.14. In particular, our heuristic suggests that the stability index derived in Section 3.3 does not yield any information concerning the existence of unstable point spectrum of the corresponding linearized operator. This motivation is further supported noting from the Evans function output along the real line in Figure 7(b) that $D'(0) > 0$, and hence $\mathrm{sgn}\partial_c d(c, q) < 0$ by Lemma 3.11 as expected.

In order to further study the point spectrum of the corresponding linearized operator, we need a high frequency bound on the eigenvalues of (3.1). By using the numerically computed profile to evaluate the functions $a_j$ in (4.26), an application of Corollary 4.3 implies that any unstable roots of $D(\lambda)$, if they exist for the given parameter values, must satisfy the bound $|\lambda| < 308$. In Figure 7(c) and (d) the output of the Evans function evaluated on a semi-circle of outer radius 308 and inner radius $10^{-3}$, from which we compute that the winding number (5.2) is equal to zero[11]. In particular, it follows that the linearized eigenvalue problem in consideration has stable point spectrum as expected. As noted in the introduction, this example is notable as being the first example of a second-order hyperbolic-parabolic conservation or balance law which admits a solitary wave with stable point spectrum.

**Remark 5.1.** *The eigenvalue estimates of Corollary 4.3 should be contrasted with the results of a convergence study based on* (4.30)*. In the example considered here, the results of a high frequency convergence study are listed below, with "Relative Error" denoting the maximum relative error between the numerically computed value of* $D(\lambda)$ *and an approximant* (4.30)

[11] In this example, the Evans function was evaluated on the contour with 3457 mesh points, yielding a maximum relative error between mesh points of 0.2. As stated before, this is sufficient to yield an accurate winding number by Rouché's Theorem.

*determined by curve fitting on the semicircle* $|\lambda| = R$, $\Re\lambda \geq 0$*:*

| *Relative Error* | *Radius* $R$ |
|---|---|
| 0.1112 | 8192 |
| 0.1525 | 4096 |
| 0.2062 | 2048 |
| 0.2740 | 1020 |
| 0.4230 | 308 |
| 0.4522 | 250 |
| 0.5484 | 130 |

*The radius* $R = 308$ *derived from our high frequency asymptotics and tracking in Corollary 4.3 thus correspond to a relative error of approximately* 0.4230*, and hence the estimates in Corollary 4.3 are quite efficient even though they produce a radius that is relatively large. Furthermore, from this convergence study it seems then that the convergence rate of* $\mathcal{O}(|\lambda|^{-1/2})$ *from* (4.30) *breaks down for* $R \approx 250$*. This suggests that the bound of* $R = 308$ *obtained from our tracking estimates in Corollary 4.3 is very close to the boundary of the high frequency asymptotics.*

Next, recalling that the subcharacteristic condition reduces to $F < 4$ in this case we see that the solitary wave must have unstable essential spectrum. This is verified numerically in Figure 7(e), where again we approximated the solitary wave by a periodically extended version of itself with very large period and used package SpectrUW. However, by performing a time evolution study of the generated homoclinic profile we find that the nature of this instability appears to be convective. That is, a small perturbation leaves the original profile relatively unchanged in shape, but grows as an oscillatory time-exponentially growing Gaussian wave packet after emerging from the profile; see Figure 8. For this numerical study, we used a Crank-Nicholson finite difference scheme, i.e. we used a forward difference time derivative and a centered, averaged spatial derivative approximation. This solitary wave is thus seen to be metastable in the sense that the perturbed solitary wave propagates relatively unchanged down the ramp, while shedding oscillatory instabilities in its wake. In the next section, we further examine this phenomenon and its relation to the stability of nearby periodic waves.

# 6 Dynamical stability and stabilization of unstable waves

As noted in the introduction, similar metastable phenomena to that observed in Section 5.2.2 have been observed by Pego, Schneider, and Uecker [PSU] for the related fourth-order diffusive Kuramoto-Sivashinsky model

$$u_t + \varepsilon\partial_x^4 u + \partial_x^3 u + \varepsilon\partial_x^2 u + \frac{\partial_x u^2}{2} = 0, \tag{6.1}$$

an alternative, small-amplitude, model for thin film flow on an incline. They describe asymptotic behavior of solutions of this model as dominated by trains of solitary pulses.

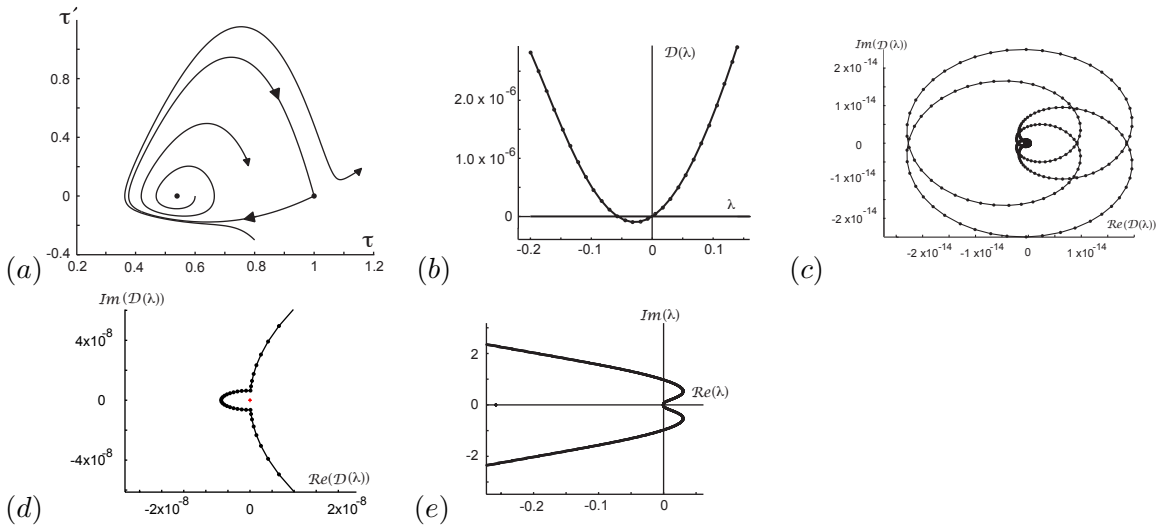


Figure 7: Evans function output for the St. Venant system with $r = 2$ and $s = 0$ corresponding to a homoclinic profile. Here $c \approx 0.7849$, $q = 1 + c$, $F = 9$, and $\nu = 0.1$. In Figure (a) we have the phase portrait plotting $\tau$ verse $\tau'$. In Figure (b) we plot the Evans function evaluated on the real line. In Figure (c) we show the Evans function output evaluated on a semicircle of radius $R = 308$ with a small inner circle of radius $10^{-3}$, where we zoom in on the origin in Figure (d). The winding number about the origin of the curve in Figure (c) is zero in these computations, yielding stability of the point spectrum. Finally, Figure (e) depicts our numerical approximation of the essential spectrum as generated by SpectrUW, demonstrating the expected essential instability.

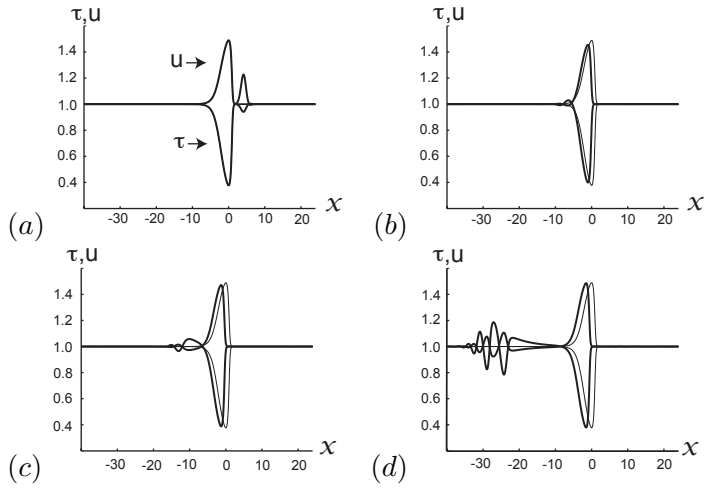


Figure 8: Time evolution snapshots for the St. Venant equations with $r = 2$, $s = 0$: all figures here are plotted as $\tau$ and $u$ vs. $x$ according to the indicated labelings. In Figure (a) we have a perturbation to the right of the profile solution. In figure (b) we see the perturbation moving left emerge from the profile and grow as oscillatory wave packets with Gaussian envelopes in Figures (c) and (d). Locally, after interaction with the perturbation, the solution seems to settle to a translate of the original profiles (thin lines). Here $c \approx 0.7849$, $q = 1 + c$, $F = 9$, and $\nu = 0.1$.

Indeed, such wave trains are easily observed on any rainy day in runoff down a rough asphalt gutter as found by many roads in the U.S. (e.g., near the last author's home), as are small oscillations between pulses as might be suggested by the analyses here and in [PSU], corresponding to convective instabilities.

Thus, both of these sets of results may be regarded as partial explanation of the somewhat surprising phenomenon that asymptotic behavior of actual inclined thin-film flow is dominated by trains of pulse solutions which are themselves unstable. Regarding this larger issue, we have a further observation that we believe completes the explanation of this interesting puzzle, at least at a level of heuristic understanding.

The key is to reformulate the question as: how can we explain observed stable behavior of trains of solitary waves that are in isolation exponentially unstable? Or, more pointedly: *how can a train of solitary pulses stabilize the convective instabilities shed from their neighbors?* Phrased in this way, the question essentially answers itself: it must be that the local dynamics of the waves are such that convected perturbations are *diminished* as they cross each solitary pulse, counterbalancing the growth experienced as they traverse the interval between pulses, on which they behave as perturbations of an unstable constant solution. This diminishing effect is clearly apparent visually in time-evolution studies; see Figure 8. However, it is a challenge to quantify it mathematically. In particular, it is only partially but not wholly encoded by the point spectrum that we usually think of as determining local dynamics of the wave [He, GZ, ZH].

Rather, the relevant entity appears to be the *dynamic spectrum*, defined as the spectrum of the periodic-coefficient linearized operator about a periodic wave obtained by gluing together copies of a suitably truncated solitary pulse. Here, the choice of truncation is not uniquely specified, but should intuitively be at a point where the wave profile has "almost converged" to its limiting endstate. This dynamic spectrum would govern the behavior of a maximally closely spaced array of solitary pulses[12], so captures the diminishing property if there is one. A bit of thought reveals the difficulty of trying to capture diminishing instead by decrease in some specified norm. For, by the analytical results of [JZN], the decay we are expecting is the diffusive decay of a solution of a heat equation[13], which does not occur at any specified rate when considered from a given norm to itself, but shows up in long-time averaged behavior from a more localized (e.g., $L^1$) norm to a less localized (e.g., $L^2$ or $L^\infty$) norm, and whose progress is difficult to measure by a "snapshot" at an intermediate stage.

In Figure 9 we depict the dynamic spectrum of the profile used in the time evolution study of Section 5.2.2, along with the periodically extended version of this profile used to carry out the necessary numerics. We see that the dynamic spectrum indeed appears to be quite stable, despite the instability of the essential spectrum of the linearized operator about the wave (corresponding to the convective instabilities discussed above), supporting our picture of pulse profiles as "de-amplifiers" that can mutually stabilize each other when

[12]That is, an array without "flat spots" but spaced sufficiently far apart that profiles do not interfere.

[13]This expectation does not come from the partially parabolic structure of the underlying problem, but from the observed "quadratic tangency" of the dynamic spectrum with the imaginary axis in Figure 9(a), corresponding to diffusive time-asymptotic behavior; see Section 1.1.2, [JZN] for further discussion.

placed in a sufficiently closely spaced wave train.

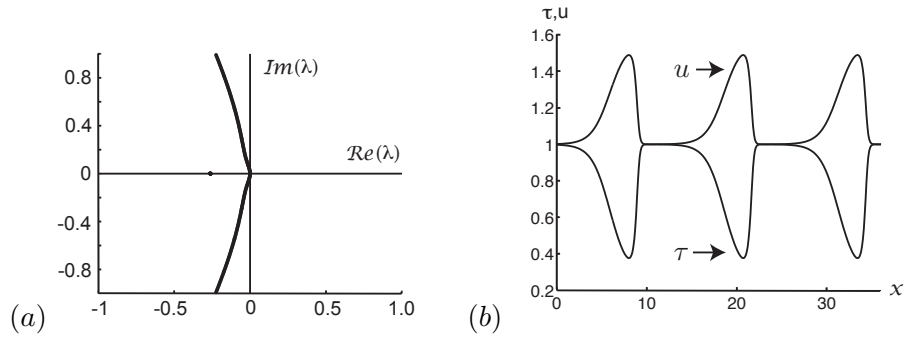


Figure 9: In Figure (a), we plot the spectrum of the periodically extended version of the profile found in Section 5.2.2 given in Figure (b). This periodic spectrum of the associated homoclinic profile is seen to be stable, in contrast to its essential spectrum which was seen to be unstable in Figure 7. This spectrum was found using again the SpectrUW package. Note that the dynamic spectrum includes also small (stable) loops close to the point spectrum of the homoclinic [G].

This suggests also that there should exist nearby periodic wave trains that are stable, despite the instability of a single solitary wave. In Figure 10, we display the spectrum and profile of an actual periodic wave (approximated like the solitary wave using MATLAB's boundary value solver) with the same period as the glued profile, showing that these are nearly identical to those of the glued profile. In particular, they appear to satisfy the spectral stability conditions shown in [JZN] to imply nonlinear modulational stability, namely: (D1) nonpositivity of the real part of the spectrum, (D2) quadratic order tangency of spectral curves at the origin, and (D3) crossing of multiplicity two of spectral curves at the origin.

More, the competition between stable dynamic spectrum encoding behavior "within" a pulse and unstable essential spectrum encoding behavior "between" pulses suggests that as the spacing between pulses is increased in a periodic array of solitary waves, or, similarly, as the period is increased in exact periodic solutions near the solitary-wave limit, the associated spectrum should become more and more unstable until the initially stable wave train transitions to instability.

In terms of the behavior suggested by the time-evolution study in Figure 8, the diminishing effect experienced by the convected perturbation as it crosses a solitary pulse should be counterbalanced by the growth it experiences as it crosses between pulses, with an exact balance achieved at some neutral spacing representing the stability transition boundary. For spacings below this neutral distance, the perturbation spends less time in growth phase, between pulses, so ultimately decays; for spacings above this distance, it spends more time, so ultimately blows up. Supporting this picture of behavior are Figures 11 and 12, the first showing the gradual decay of a perturbation crossing an array with period $X = 19.8$ and the second showing the growth and eventual explosion of a perturbation crossing an array

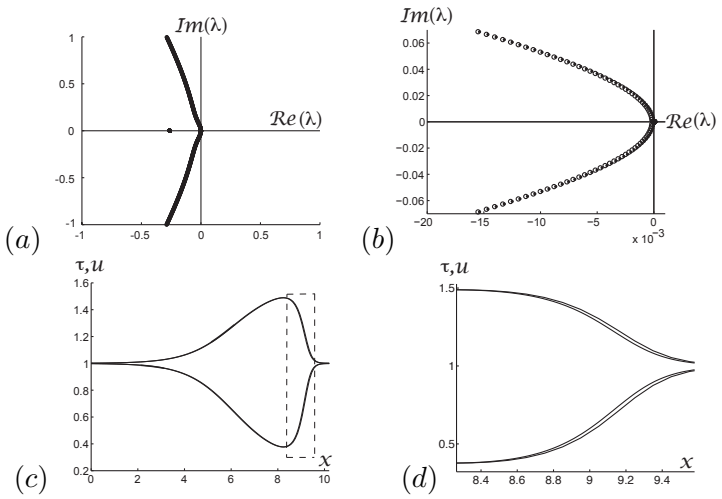


Figure 10: In Figure (a), we have superimposed the spectrum of an exact periodic traveling wave solution of (2.2) and the spectrum associated to a periodically extended version of the homoclinic profile found in Section 5.2.2 with the same period. As one can see, the spectra are nearly identical: in Figure (b) we zoom in on Figure (a) near the origin, showing the *very* slight discrepancy between the spectrum of the exact periodic (circles) and the periodically extended homoclinic (solid dots). Again, this spectrum was found using SpectrUW. Continuing, in Figure (c) we superimpose the profiles of the exact periodic traveling wave solution (bold) with the periodically extended homoclinic (thin) with the same period. Again, these profiles are nearly identical: in Figure (d) we zoom in on the dashed box in Figure (c) to illustrate the close agreement of these profiles.

with period $X = 30$. Approximation of the spectra indicates an actual stability transition at $X \approx 20.6$ consistent with these time-evolution experiments.

In companion papers [BJNRZ1, BJNRZ2], we show by more detailed numerical study that this is indeed the case, establishing spectral, linearized, and nonlinear stability of periodic wave trains in a band near the homoclinic limit. This band by continuity of spectra must extend below the period $X \approx 10$ of the glued wave from which the dynamic spectrum was computed, and in fact it extends significantly farther, down to a period $X \approx 5.4$ for which the associated periodic wave only vaguely resembles a separate array of solitary pulses; see [BJNRZ1, BJNRZ2] for further details. For comparison, the period at the Hopf bifurcation marking the lower boundary of existence of periodic profiles is $X \approx 3.9$; see Figure 3.9 in [BJNRZ2].

This mechanism by which unstable solitary waves may be "glued together" to form stable periodic waves is somewhat reminiscent of the mechanism pointed out in [SS] by which "fronts" and "backs" with stable point spectrum but unstable essential spectrum on their common side may be glued together to form exponentially stable solitary waves in which the unstable constant state is "trapped" between the front and back. However, here, where perturbations decay time-algebraically rather than time-exponentially, and are not trapped but convect across consecutive pulses, the process is somewhat more subtle. Likewise, the nonlinear stability analysis (performed in [JZN, JZ]) is here more delicate, depending on detailed Green function estimates like those used to establish stability of viscous shock waves [MaZ4, Z1], whereas nonlinear exponential stability of front/back combinations follows by standard semigroup methods [Sat, He] once there has been established the requisite spectral gap [SS].

Note that the described mechanism of stabilization does not appear to be limited to exact periodic solutions, but suggests that also a sufficiently closely spaced array of solitary waves should be stable, even an irregularly spaced array. Moreover, the fact that perturbations are convected in one direction only suggests that a sufficiently closely spaced half-infinite array, extending only in the direction of propagation, should also be stable. This last conjecture is supported by the time-evolution study displayed in Figure 13, depicting the gradual decay of a perturbation convecting to the left.

However, our analysis for the moment is limited to the periodic case, where we can apply the global, or "homogenized", estimates of [JZN]. We point to exploration of the link between dynamic spectrum and local behavior, or similar quantification of de-amplification properties, as an interesting direction for further development; see [BJNRZ2] for further discussion of this and related topics. As noted earlier, the fact that decay experienced by perturbations while crossing pulses appears to be diffusive, or "spreading", rather than time-exponential, or "shrinking", makes this a tricky problem, and distinguishes it from cases already treated; in particular, we do not see at the moment a simple norm that can play the role of the weighted norms in [SS] and record the decay experienced when crossing a single pulse.

Another interesting direction for future study, and one that might be a first step in treating irregular patterns, would be to obtain pointwise Green function bounds as in

[JZN, MaZ3] about a single metastable pulse, generalizing the bounds obtained in [OZ1] for perturbations of unstable constant solutions. A related problem is to obtain rigorous nonlinear instability results in the metastable case. (Recall that essential instability does not immediately imply nonlinear instability due to the absence of a spectral gap.)

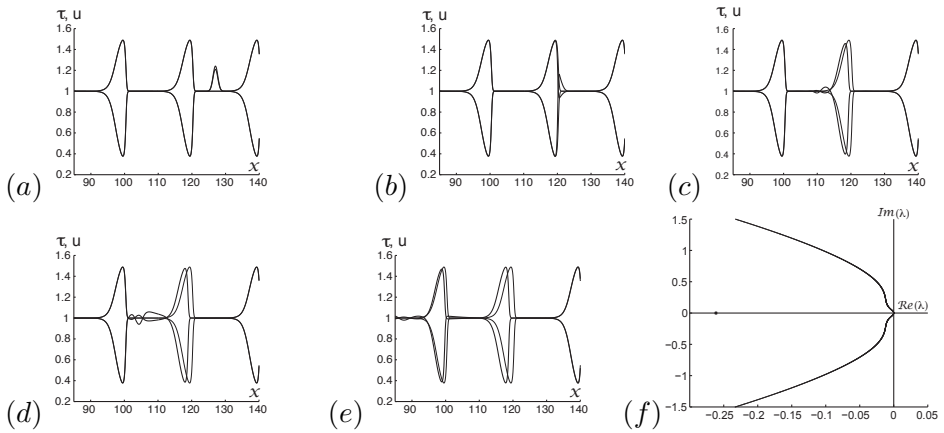


Figure 11: Time evolution snapshots for a periodically extended version of the homoclinic orbit found in Section 5.2.2, here taken with period $X = 19.8$, corresponding to the St. Venant equations with $(r, s) = (2, 0)$and $c \approx 0.7849$, $q = 1 + c$, $F = 9$, and $\nu = 0.1$. In Figure (a) we have the initial perturbation between two copies of the homoclinic. In Figure (b), the perturbation moves to the left and becomes de-amplified through the pulse, reemerging in Figures (c) and (d) with smaller amplitude. The perturbation then continues to the left through the second pulse and begins to emerge with significantly diminished amplitude in Figure (e). In Figure (f), we show our numerical approximation (computed with SpectrUW) of the spectrum of the linearizied operator about this periodically extended homoclinic, which here appears to be quite stable as compared to the unstable spectrum of the actual homoclinic depicted in Figure 7(e). As in Figure 8, it appears that, locally, the perturbed periodically extended wave converges to a translate of the original profile, indicating stability.

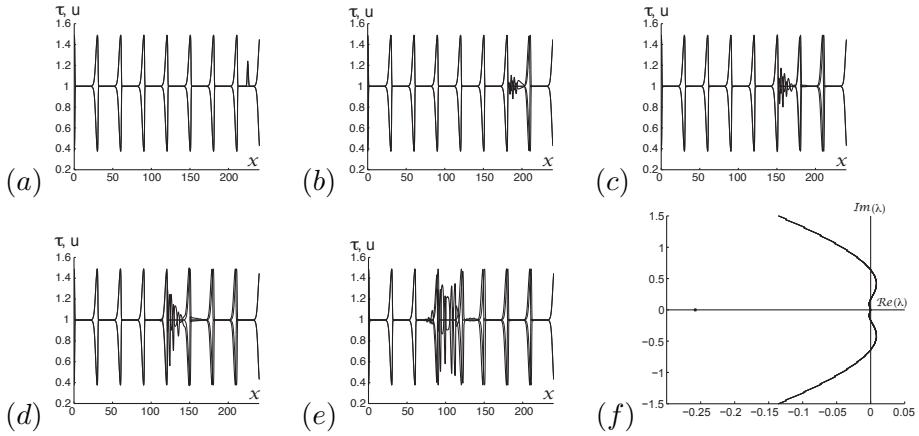


Figure 12: Time evolution snapshots for a periodically extended version of the homoclinic orbit found in Section 5.2.2, here taken with period $X = 30$, corresponding to the St. Venant equations with $(r, s) = (2, 0)$and $c \approx 0.7849$, $q = 1 + c$, $F = 9$, and $\nu = 0.1$. In Figure (a) we have the initial perturbation between two copies of the homoclinic. In Figures (b)-(e), the perturbation moves through consecutive pulses. In this case, the perturbation spends "too much time" in the unstable constant state resulting in the convected instability being too strong for the de-amplification effect of the pulse to stabilize the solution. In Figure (f), we show our numerical approximation (computed with SpectrUW) of the spectrum of the linearizied operator about this periodically extended homoclinic, clearly demonstrating the instability observed in Figures (a)-(e).

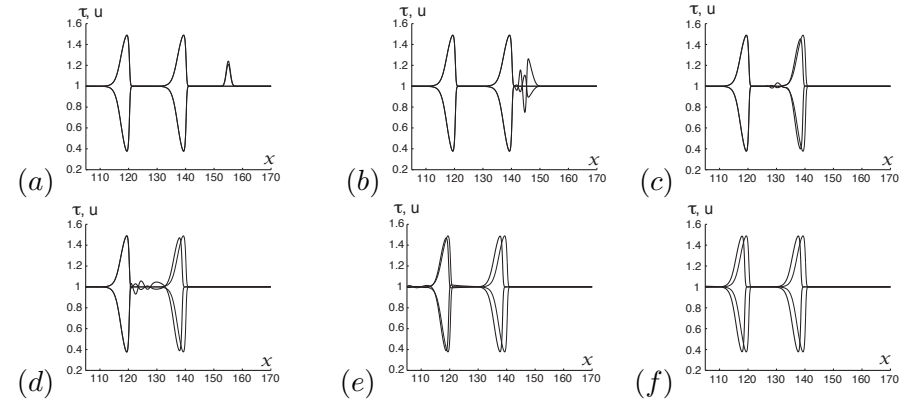


Figure 13: Time evolution snapshots for an extended version of the homoclinic orbit found in Section 5.2.2,corresponding to the St. Venant equations with $(r, s) = (2, 0)$and $c \approx 0.7849$, $q = 1 + c$, $F = 9$, and $\nu = 0.1$. Here, the extension is taken to be periodic with period $X = 19.8$ in a half-infinite array. As in the case of the infinite array study in Figure 11, this half-infinite array seems to be quite stable.

# A High Frequency Bounds

Here, we record the quantities necessary to compute the high frequency bounds of Corollary 4.3 in terms of the original homoclinic orbit and of quantity $\bar{\alpha}$ defined in (3.3).

$$\Theta^0_{++} = \begin{pmatrix} \frac{\bar{\alpha}\bar{\tau}^2}{c\nu} & -\frac{\bar{\tau}^2}{\nu} \\ -\frac{\bar{\alpha}\bar{\tau}^2}{2\nu} & \frac{\bar{\tau}'}{\bar{\tau}} - \frac{c\bar{\tau}^2}{2\nu} \end{pmatrix}, \quad \Theta^1_{+-} = \begin{pmatrix} -\frac{2\bar{\tau}'}{\sqrt{\nu}} + \frac{\bar{\tau}^3}{\nu^{3/2}}(\frac{\bar{\alpha}}{c} + c) \\ -\frac{r\bar{\tau}^{s+2}(q-c\bar{\tau})^{r-1}}{2\sqrt{\nu}} - \frac{\bar{\alpha}}{2}\frac{\bar{\tau}^3}{\nu^{3/2}} \end{pmatrix},$$

$$\Theta^1_{++} = \begin{pmatrix} 0 & -\frac{2\bar{\tau}'}{\sqrt{\nu}} + \frac{\bar{\tau}^3}{\nu^{3/2}}(\frac{\bar{\alpha}}{c} + c) \\ \frac{\bar{\tau}}{2\sqrt{\nu}}\left((s+1)\bar{\tau}^s(q-c\bar{\tau})^r + c\bar{\alpha}\frac{\bar{\tau}^2}{\nu}\right) & \frac{r\bar{\tau}^{s+2}(q-c\bar{\tau})^{r-1}}{2\sqrt{\nu}} + \frac{\bar{\alpha}}{2}\frac{\bar{\tau}^3}{\nu^{3/2}} \end{pmatrix},$$

$$\Theta^2_{++} = \begin{pmatrix} -\frac{(s+1)\bar{\tau}^{s+2}(q-c\bar{\tau})^r}{\nu} - \frac{c\bar{\alpha}}{\sqrt{\nu}}\frac{\bar{\tau}^3}{\nu^{3/2}} & -\frac{r\bar{\tau}^{s+3}(q-c\bar{\tau})^{r-1}}{\nu} \\ 0 & \frac{(s+1)\bar{\tau}^{s+2}(q-c\bar{\tau})^r}{2\nu} + \frac{c\bar{\alpha}}{2\sqrt{\nu}}\frac{\bar{\tau}^3}{\nu^{3/2}} \end{pmatrix},$$

$$\Theta^3_{++} = \begin{pmatrix} 0 & -\frac{(s+1)\bar{\tau}^{s+3}(q-c\bar{\tau})^r}{\nu^{3/2}} - \frac{c\bar{\alpha}}{\sqrt{\nu}}\frac{\bar{\tau}^4}{\nu^2} \\ 0 & 0 \end{pmatrix}, \quad \Theta^0_{+-} = \begin{pmatrix} \frac{\bar{\tau}^2}{\nu} \\ \frac{\bar{\tau}'}{2\bar{\tau}} - \frac{c}{2}\frac{\bar{\tau}^2}{\nu} \end{pmatrix},$$

$$\Theta^2_{+-} = \begin{pmatrix} \frac{r\bar{\tau}^{s+3}(q-c\bar{\tau})^{r-1}}{\nu} \\ \frac{(s+1)\bar{\tau}^{s+2}(q-c\bar{\tau})^r}{2\nu} + \frac{c\bar{\alpha}}{2\sqrt{\nu}}\frac{\bar{\tau}^3}{\nu^{3/2}} \end{pmatrix}, \quad \Theta^3_{+-} = \begin{pmatrix} -\frac{(s+1)\bar{\tau}^{s+3}(q-c\bar{\tau})^r}{\nu^{3/2}} - \frac{c\bar{\alpha}}{\sqrt{\nu}}\frac{\bar{\tau}^4}{\nu^2} \\ 0 \end{pmatrix},$$

$$\Theta^0_{-+} = \begin{pmatrix} \frac{\bar{\alpha}\bar{\tau}^2}{2\nu} & \frac{\bar{\tau}'}{\bar{\tau}} - \frac{c\bar{\tau}^2}{2\nu} \end{pmatrix}, \quad \Theta^2_{-+} = \begin{pmatrix} 0 & \frac{(s+1)\bar{\tau}^{s+2}(q-c\bar{\tau})^r}{2\nu} + \frac{c\bar{\alpha}}{2\sqrt{\nu}}\frac{\bar{\tau}^3}{\nu^{3/2}} \end{pmatrix},$$

$$\Theta^1_{-+} = \begin{pmatrix} \frac{\bar{\tau}}{2\sqrt{\nu}}\left((s+1)\bar{\tau}^s(q-c\bar{\tau})^r + c\bar{\alpha}\frac{\bar{\tau}^2}{\nu}\right) & \frac{r\bar{\tau}^{s+2}(q-c\bar{\tau})^{r-1}}{2\sqrt{\nu}} + \frac{\bar{\alpha}}{2}\frac{\bar{\tau}^3}{\nu^{3/2}} \end{pmatrix}, \quad \Theta^0_{--} = \begin{pmatrix} \frac{\bar{\tau}'}{\bar{\tau}} - \frac{c\bar{\tau}^2}{2\nu} \end{pmatrix},$$

$$\Theta^1_{--} = \begin{pmatrix} -\frac{(s+1)\bar{\tau}^{s+2}(q-c\bar{\tau})^r}{2\nu} + \frac{c\bar{\alpha}}{2\sqrt{\nu}}\frac{\bar{\tau}^3}{\nu^{3/2}} \end{pmatrix}, \quad \Theta^2_{--} = \begin{pmatrix} \frac{(s+1)\bar{\tau}^{s+2}(q-c\bar{\tau})^r}{2\nu} + \frac{c\bar{\alpha}}{2\sqrt{\nu}}\frac{\bar{\tau}^3}{\nu^{3/2}} \end{pmatrix}.$$

# References


[AGJ] J. Alexander, R. Gardner and C.K.R.T. Jones, *A topological invariant arising in the analysis of traveling waves*, J. Reine Angew. Math. 410 (1990) 167–212.

[AMPZ1] A. Azevedo, D. Marchesin, B. Plohr and K. Zumbrun, *Bifurcation from the constant state of nonclassical viscous shock waves,* Comm. Math. Phys. 202 (1999) 267–290.

[AMPZ2] A. Azevedo, D. Marchesin, B. Plohr and K. Zumbrun, *Long-lasting diffusive solutions for systems of conservation laws.* VI Workshop on Partial Differential Equations, Part I (Rio de Janeiro, 1999). Mat. Contemp. 18 (2000), 1–29.

[BM] N.J. Balmforth and S. Mandre, *Dynamics of roll waves,* J. Fluid Mech. 514 (2004) 1–33.

[BN] D. Bresch and P. Noble, *Mathematical derivation of viscous shallow-water equations with zero surface tension,* preprint (2010).

[BHZ] B. Barker, J. Humpherys, and K. Zumbrun, *One-dimensional stability of parallel shock layers in isentropic magnetohydrodynamics,* Journal of Differential Equations, 249(2010), 2175-2213.

[BLZ] B. Barker, O. Lafitte, and K. Zumbrun, *Existence and stability of viscous shock profiles for 2-D isentropic MHD with infinite electrical resistivity*, Acta Mathematica Scientia, 30 (2010), 447–498

[BJNRZ1] B. Barker, M. Johnson, P. Noble, M. Rodrigues, and K. Zumbrun, *Spectral stability of periodic viscous roll waves*, in preparation:

[BJNRZ2] B. Barker, M. Johnson, P. Noble, M. Rodrigues, and K. Zumbrun, *Witham averaged equations and modulational stability of periodic solutions of hyperbolic-parabolic balance laws,* Journées équations aux dérivées partielles (2010), Exp. No. 3, 24 pages.

[Br] L. Q. Brin, *Numerical testing of the stability of viscous shock waves.* Math. Comp. 70 (2001) 235, 1071–1088.

[BrZ] L. Brin and K. Zumbrun, *Analytically varying eigenvectors and the stability of viscous shock waves.* Seventh Workshop on Partial Differential Equations, Part I (Rio de Janeiro, 2001). Mat. Contemp. 22 (2002), 19–32.

[CuD] C. Curtis and B. Deconick, *On the convergence of Hill's method*, Mathematics of computation 79, 169–187, 2010.

[CDKK] J. D. Carter, B. Deconick, F. Kiyak, and J. Nathan Kutz, *SpectrUW: a laboratory for the numerical exploration of spectra of linear operators*, Mathematics and Computers in Simulation 74, 370–379, 2007.

[CD] H-C. Chang and E.A. Demekhin, *Complex wave dynamics on thin films,* (Elsevier, 2002).

[DK] B. Deconinck and J. Nathan Kutz, *Computing spectra of linear operators using Hill's method,* J. Comp. Physics 219, 296–321, 2006.

[D] R. Dressler, *Mathematical solution of the problem of roll waves in inclined open channels,* CPAJM (1949) 149–190.

[G] R. Gardner, *On the structure of the spectra of periodic traveling waves*, J. Math. Pures Appl. 72 (1993), 415-439.

[GZ] R. Gardner and K. Zumbrun, *The Gap Lemma and geometric criteria for instability of viscous shock profiles*, Comm. Pure Appl. Math. 51 (1998), no. 7, 797–85.

[Go] P. Godillon, *Linear stability of shock profiles for systems of conservation laws with semi-linear relaxation,* Phys. D, 148 (2001), no. 3-4, 289–316.

[He] D. Henry, *Geometric theory of semilinear parabolic equations*, Lecture Notes in Mathematics, Springer–Verlag, Berlin (1981).

[HZ] P. Howard and K. Zumbrun, *Stability of undercompressive shocks,* J. Differential Equations 225 (2006) 308–360.

[HuZ] J. Humpherys and K. Zumbrun, *An efficient shooting algorithm for Evans function calculations in large systems,* Phys. D 220 (2006), no. 2, 116–126.

[HC] S.-H. Hwang and H.-C. Chang, *Turbulent and inertial roll waves in inclined film flow,* Phys. Fluids 30 (1987), no. 5, 1259–1268.

[HLZ] J. Humpherys, O. Lafitte, and K. Zumbrun, *Stability of viscous shock profiles in the high Mach number limit,* Comm. Math. Phys. 293 (2010), no. 1, 1–36.

[HLyZ1] J. Humpherys, G. Lyng, and K. Zumbrun, *Spectral stability of ideal-gas shock layers*, Arch. Ration. Mech. Anal. 194 (2009), no. 3, 1029–1079.

[HLyZ2] J. Humpherys, G. Lyng, and K. Zumbrun, *Multidimensional spectral stability of large-amplitude Navier–Stokes shocks,* in preparation.

[JK] S. Jin and M.A. Katsoulakis, *Hyperbolic Systems with Supercharacteristic Relaxations and Roll Waves,* SIAM J. Applied Mathematics 61 (2000), 273-292.

[JZ] M. Johnson and K. Zumbrun, *Nonlinear stability of periodic traveling waves of viscous conservation laws in the generic case*, J. Diff. Eq. 249 (2010) no. 5, 1213-1240.

[JZN] M. Johnson, K. Zumbrun, and P. Noble, *Nonlinear stability of viscous roll waves,* to appear in SIAM Journal on Mathematical Analysis.

[K] T. Kato, *Perturbation theory for linear operators*, Springer–Verlag, Berlin Heidelberg (1985).

[KL] J. Kierzenka and L. F. Shampine, A BVP solver that controls residual and error. J. Numer. Anal. Ind. Appl. Math., 3(1-2):27–41, 2008.

[LRTZ] G. Lyng, M. Raoofi, B. Texier, and K. Zumbrun, *Pointwise Green function bounds and stability of combustion waves,* J. Differential Equations 233 (2007), no. 2, 654–698.

[MaZ1] C. Mascia and K. Zumbrun, *Pointwise Green's function bounds and stability of relaxation shocks,* Indiana Univ. Math. J. 51 (2002), no. 4, 773–904.

[MaZ3] C. Mascia and K. Zumbrun, *Pointwise Green function bounds for shock profiles of systems with real viscosity.* Arch. Ration. Mech. Anal. 169 (2003), no. 3, 177–263.

[MaZ4] C. Mascia and K. Zumbrun, *Stability of large-amplitude viscous shock profiles of hyperbolic-parabolic systems,* Arch. Ration. Mech. Anal. 172 (2004), no. 1, 93–131.

[MeZ] G. Métivier and K. Zumbrun, *Large viscous boundary layers for noncharacteristic nonlinear hyperbolic problems,* Mem. Amer. Math. Soc. 175 (2005), no. 826, vi+107 pp.

[N1] P. Noble, *On the spectral stability of roll waves,* Indiana Univ. Math. J. 55 (2006) 795–848.

[N2] P. Noble, *Linear stability of viscous roll waves,* Comm. Partial Differential Equations 32 (2007) no. 10-12, 1681–1713.

[NR] P. Noble, and M. Rodrigues, *Modulated wave trains in generalized Kuramoto-Sivashinksi equations,* preprint (2010).

[OZ1] M. Oh and K. Zumbrun, *Stability of periodic solutions of viscous conservation laws with viscosity- 1. Analysis of the Evans function*, Arch. Ration. Mech. Anal. 166 (2003), no. 2, 99–166.

[PSU] R. Pego, H. Schneider, and H. Uecker, *Long-time persistence of Korteweg-de Vries solitons as transient dynamics in a model of inclined film flow,* Proc. Royal Soc. Edinburg 137A (2007) 133–146.

[PW1] R. L. Pego and M. I. Weinstein, *Asymptotic Stability of Solitary Waves*, Commun. Math. Phys. 164 (1994), 305-349.

[PW2] R. L. Pego and M.I. Weinstein, *Eigenvalues, and instabilities of solitary waves*, Philos. Trans. Roy. Soc. London Ser. A 340 (1992), 47–94.

[PZ] Plaza, R. and Zumbrun, K., *An Evans function approach to spectral stability of small-amplitude shock profiles*, J. Disc. and Cont. Dyn. Sys. 10. (2004), 885-924.

[RZ] M. Raoofi and K. Zumbrun, *Stability of undercompressive viscous shock profiles of hyperbolic-parabolic systems,* J. Diff. Eq. 246 (2009) 1539–1567.

[SS] B. Sandstede and A. Scheel *Gluing unstable fronts and backs together can produce stable pulses,* Nonlinearity 13 (2000), no. 5, 1465–1482.

[Sat] D. Sattinger, *On the stability of waves of nonlinear parabolic systems.* Adv. Math. 22 (1976) 312–355.

[TZ1] B. Texier and K. Zumbrun, *Transition to longitudinal instability of detonation waves is generically associated with Hopf bifurcation to time-periodic galloping solutions,* Communications in Mathematical Physics 302 (2011), 1–51.

[TZ2] B. Texier and K. Zumbrun, *Relative Poincaré-Hopf bifurcation and galloping instability of traveling waves,* Methods Appl. Anal. 12 (2005), no. 4, 349–380.

[W] H. A. Win, *Model equation of surface waves of viscous fluid down an inclined plane,* Journal of Mathematics of Kyoto University 33 (1993), no. 4, 803–824.

[YKH] J. Yu, J. Kevorkian, and R. Haberman, *Weak nonlinear long waves in channel flow with internal dissipation*, Studies in Applied Mathematics 105 (2000), no. 2, 143–163.

[Z1] K. Zumbrun, *Stability of large-amplitude shock waves of compressible Navier–Stokes equations,* with an appendix by Helge Kristian Jenssen and Gregory Lyng, in Handbook of mathematical fluid dynamics. Vol. III, 311–533, North-Holland, Amsterdam, (2004).

[Z2] K. Zumbrun, *Dynamical stability of phase transitions in the p-system with viscosity-capillarity*, SIAM J. Appl. Math. 60 (2000), 1913-1929.

[Z3] K. Zumbrun, *Planar stability criteria for viscous shock waves of systems with real viscosity*, in Hyperbolic systems of balance laws, P. Marcati, ed., vol. 1911 of Lecture Notes in Math., Springer, Berlin, 2007, pp. 229–326.

[Z4] K. Zumbrun, *Multidimensional stability of planar viscous shock waves.* Advances in the theory of shock waves, 307–516, Progr. Nonlinear Differential Equations Appl., 47, Birkhäuser Boston, Boston, MA, 2001.

[Z5] K. Zumbrun, *Stability of detonation waves in the ZND limit,* to appear, Arch. Rat. Mech. Anal.

[Z6] K. Zumbrun, *Numerical error analysis for evans function computations: a numerical gap lemma, centered-coordinate methods, and the unreasonable effectiveness of continuous orthogonalization,* to appear in SIAM Journal on Applied Dynamicsl Systems.

[Z8] K. Zumbrun, *Center stable manifolds for quasilinear parabolic pde and conditional stability of nonclassical viscous shock waves*, preprint (2008).

[Z9] K. Zumbrun, *Conditional stability of unstable viscous shock waves in compressible gas dynamics and MHD*, preprint (2009).

[Z10] K. Zumbrun, *Stability and dynamics of viscous shock waves,* Proceedings, 2009 IMA summer school on conservation laws, Springer, (2010).

[ZH] K. Zumbrun and P. Howard, *Pointwise semigroup methods and stability of viscous shock waves,* Indiana Univ. Math. J. 47 (198) 741–871.